




# JGR Atmospheres

## RESEARCH ARTICLE

10.1029/2019JD032191

## A Model for Turbulence Spectra in the Equilibrium Range of the Stable Atmospheric Boundary Layer

Yu Cheng<sup>1</sup> , Qi Li<sup>2</sup>, Stefania Argentini<sup>3</sup>, Chadi Sayde<sup>4</sup> , and Pierre Gentine<sup>1</sup> 

<sup>1</sup>Department of Earth and Environmental Engineering, Columbia University, New York, NY, USA, <sup>2</sup>School of Civil and Environmental Engineering, Cornell University, Ithaca, NY, USA, <sup>3</sup>Institute of Atmospheric Sciences and Climate, CNR, Rome, Italy, <sup>4</sup>Department of Biological and Agricultural Engineering, North Carolina State University at Raleigh, Raleigh, NC, USA

### Key Points:

- Turbulent kinetic energy and temperature spectra in horizontal wavenumber consist of three regions in the stable ABL
- Large-scale separation is required for numerical simulations to resolve the transition region
- Monin-Obukhov similarity theory may not apply in the very stable ABL as the buoyancy scale is not considered

### Supporting Information:

- Supporting Information S1

### Correspondence to:

Y. Cheng,  
yc2965@columbia.edu

### Citation:

Cheng, Y., Li, Q., Argentini, S., Sayde, C., & Gentine, P. (2020). A model for turbulence spectra in the equilibrium range of the stable atmospheric boundary layer. *Journal of Geophysical Research: Atmospheres*, 125, e2019JD032191. <https://doi.org/10.1029/2019JD032191>

Received 5 DEC 2019

Accepted 17 FEB 2020

Accepted article online 20 FEB 2020

**Abstract** Stratification can cause turbulence spectra to deviate from Kolmogorov's isotropic  $-5/3$  power law scaling in the universal equilibrium range at high Reynolds numbers. However, a consensus has not been reached with regard to the exact shape of the spectra. Here we propose a shape of the turbulent kinetic energy and temperature spectra in horizontal wavenumber for the equilibrium range that consists of three regimes at small Froude number: the buoyancy subrange, a transition region, and the isotropic inertial subrange through dimensional analysis and substantial revision of previous theoretical approximation. These spectral regimes are confirmed by various observations in the atmospheric boundary layer. The representation of the transition region in direct numerical simulations will require large-scale separation between the Dougherty-Ozmidov scale and the Kolmogorov scale for strongly stratified turbulence at high Reynolds numbers, which is still challenging computationally. In addition, we suggest that the failure of Monin-Obukhov similarity theory in the very stable atmospheric boundary layer is due to the fact that it does not consider the buoyancy scale that characterizes the transition region.

## 1. Introduction

The velocity spectra of isotropic turbulence follow a  $-5/3$  power law scaling in the inertial subrange (Kolmogorov, 1941). However, stratification (Lilly, 1983) is widely observed in geophysical turbulence, for example, in the nocturnal atmospheric boundary layer (ABL) (Mahrt, 1998), in most part of the troposphere (Fiedler & Panofsky, 1970), above the tropopause (Nastrom & Gage, 1985; Tulloch & Smith, 2006), and below the ocean mixed layer (Baker & Gibson, 1987) and generates anisotropy. Because of this stratification (Bolgiano, 1959; Dougherty, 1961; Lumley, 1964; Phillips, 1965; Weinstock, 1978), the spectra deviate from the  $-5/3$  scaling of isotropic turbulence. It is worth noting that the Dougherty-Ozmidov scale (Dougherty, 1961; Ozmidov, 1965) has been suggested (Gargett et al., 1984; Grachev et al., 2015; Lang & Waite, 2019; Li et al., 2016; Waite, 2011) to characterize the largest scale of isotropic turbulence under stratification, below which the isotropic  $-5/3$  scaling is still expected.

In the mesoscale regime, a spectral scaling close to  $-5/3$  is also observed (Nastrom & Gage, 1985) in horizontal wavenumber, which, however, should not be explained by Kolmogorov's isotropic turbulence hypothesis (Riley & Lindborg, 2008). An inverse cascade of energy from small to large scales (Lilly, 1983; Gage & Nastrom, 1986) was proposed to explain this  $-5/3$  scaling at lower wavenumbers but was not supported by observations in the upper troposphere (Cho & Lindborg, 2001) or numerical simulations of forced stratified turbulence (Herring & Métais, 1989). Recently, a hypothesis of direct energy cascade from large to small scales (Lindborg, 2006) was supported by direct numerical simulation (DNS) studies (Brethouwer et al., 2007; Kimura & Herring, 2012; Riley & DeBruynkops, 2003; Waite & Bartello, 2004) to explain the  $-5/3$  scaling of anisotropic turbulence under stratification. Lindborg (2006) suggested that the direct energy cascade and the  $-5/3$  scaling of anisotropic turbulence could hold for the Dougherty-Ozmidov scale. However, Waite (2011) showed using large-eddy simulations (LES) that the stratified turbulence cascade breaks down at the buoyancy scale (Billant & Chomaz, 2001; Waite, 2011), which represents the thickness of the shear layers (Waite & Bartello, 2004) in stratified turbulence and is larger than the Dougherty-Ozmidov scale. In particular, Waite (2011) reported a spectral slope shallower than  $-5/3$  below the buoyancy scale, that is, a spectral bump, which was also observed in other numerical studies (Augier et al., 2015; Brethouwer et al., 2007; Maffioli & Davidson, 2016).

In the atmospheric surface layer (i.e., roughly the lowest 10% of the ABL; Stull, 1988), and thus at high Reynolds numbers, it is widely accepted that Monin-Obukhov similarity theory (MOST) (Monin & Obukhov, 1954) works well in neutral or weakly stable cases but does not apply in very stable cases (Mahrt, 1998, 2014). Several hypotheses have been proposed to account for the failure of MOST in the very stable ABL, such as mesoscale motions (Mahrt, 1999; Smeets et al., 1998), surface heterogeneity (Derbyshire, 1995), and Kelvin-Helmholtz instability with discontinuous and intermittent turbulence (Cheng et al., 2005). MOST has been applied to calculate turbulent fluxes from the stability parameter defined by the measurement height (distance to the wall) and the Obukhov length (Obukhov, 1946). It is possible that some other parameter (e.g., length scale) might be missing in MOST (Tong & Ding, 2019; Tong & Nguyen, 2015) as it cannot entirely explain stably stratified turbulence in the ABL.

Below the energy-containing range, Kolmogorov (1941) suggested that the statistics of small-scale motions have a universal form in the “universal equilibrium range” (Pope, 2000). However, under stratification, turbulent motions with length scales below the energy-containing range will depend on the stratification strength so that the statistics may not be “universal.” We thus denote scales below the energy-containing range as being in the “equilibrium range” for stably stratified turbulence in this manuscript. Weinstock (1978) derived the spectral scaling of turbulent kinetic energy (TKE) by assuming “approximately isotropic” turbulence under stratification; that is, (1) vertical velocity  $w$  spectrum is proportional to horizontal velocity  $u$  spectrum across wavenumbers in the equilibrium range and (2) turbulence spectrum in vertical wavenumber  $k_3$  is the same as that in horizontal wavenumber  $k_1$ . Yet it is now well known that this isotropy assumption has to be incorrect. For eddies below energy-containing scales in the ABL, we thus relax the “approximately isotropic” assumption and conduct spectral analysis for both isotropic and anisotropic turbulence in the equilibrium range. Dimensional analysis and theoretical models for TKE and temperature spectra in horizontal wavenumber  $k_1$  are introduced in section 2. Besides, the differences in theoretical approximation between Weinstock (1978) and this study are emphasized in the supporting information. Various field observations in the stably stratified ABL, DNS of stably stratified Ekman layer, and interpretations of results are elaborated in section 3. This study then concludes in section 4.

## 2. Dimensional Analysis and Spectral Approximation

### 2.1. Length Scale Definition

The strength of the stratification is assessed using the horizontal Froude number  $Fr_h = \frac{U}{NL_H}$ , where  $U$  is root mean square of the horizontal velocity (magnitude of the horizontal velocity),  $N$  is the Brunt-Väisälä frequency, and  $L_H$  is a horizontal length scale. In the limit of very strong stratification,  $Fr_h \rightarrow 0$ . The horizontal length scale  $L_H = \frac{U^3}{\epsilon}$  follows the definition in Brethouwer et al. (2007), where  $\epsilon$  is the TKE dissipation rate. Detailed support and analyses for the definition of  $L_H$  can be found in Maffioli and Davidson (2016). The Reynolds number is  $Re = \frac{UL_H}{\nu}$ , where  $\nu$  is the kinematic viscosity and the buoyancy Reynolds number is  $Re_b = ReFr_h^2$ , which characterizes the ratio of the vertical advection and diffusion terms (Brethouwer et al., 2007).

The buoyancy scale (Billant & Chomaz, 2001) is related to the overturning of internal gravity waves (Carnevale et al., 2001; Waite & Bartello, 2006) and represents the thickness of the shear layers (Waite & Bartello, 2004) in stratified turbulence. In particular, previous studies (Augier et al., 2015; Brethouwer et al., 2007; Maffioli & Davidson, 2016; Waite, 2011) reported a spectral bump around the buoyancy scale, which seems to be connected to Kelvin-Helmholtz instabilities (Brethouwer et al., 2007; Laval et al., 2003; Waite, 2011). By definition, the buoyancy length scale is  $L_b = 2\pi \frac{U}{N}$  (Billant & Chomaz, 2001; Waite, 2011), and the corresponding wavenumber is

$$k_b = \frac{2\pi}{L_b}. \quad (1)$$

The Dougherty-Ozmidov length scale is  $L_O = 2\pi \left( \frac{\epsilon}{N^3} \right)^{1/2}$  (Dougherty, 1961; Ozmidov, 1965) and can be regarded as the outer scale for isotropic turbulence (Gargett et al., 1984; Grachev et al., 2015; Lang & Waite, 2019; Li et al., 2016; Waite, 2011). The wavenumber corresponding to the Dougherty-Ozmidov length scale is

$$k_O = \frac{2\pi}{L_O}. \quad (2)$$

As Dougherty and Ozmidov independently defined this length scale, we call it Dougherty-Ozmidov scale following Grachev et al. (2015). We thus assume that isotropic turbulence applies only for length scales below  $L_O$  when there is no wall. Strict “local isotropy” condition requires the  $-5/3$  scaling plus that the ratio of cross-stream to streamwise spectra to be  $4/3$  (Pope, 2000). Gargett et al. (1984) reported that the ratio of cross-stream to streamwise spectra is close to  $4/3$  below the Dougherty-Ozmidov scale in stratified turbulence. Biltoft (2001) reported that the ratio of lateral to longitudinal velocity component spectra approaches 1 in the stable ABL. Chamecki and Dias (2004) reported that the ratio of vertical to streamwise spectra is smaller than  $4/3$  but the deviation is not large at stable conditions. Here we assume that turbulence is isotropic below the Dougherty-Ozmidov scale without referring to the strict  $4/3$  ratio as it is not always observed even though the deviation might not be too significant.

The ratio of the buoyancy scale to Dougherty-Ozmidov scale is related to the horizontal Froude number as  $\frac{L_b}{L_O} = Fr_h^{-1/2}$ . Therefore, small  $Fr_h$  ( $Fr_h \ll 1$ ) is required for a scale separation between  $L_b$  and  $L_O$ , which is possible in the ABL since the strongly stratified conditions can be observed (Mahrt, 1998). The Kolmogorov length scale (Kolmogorov, 1941) is  $\eta = (\nu^3/\epsilon)^{1/4}$  and corresponds to the wavenumber  $k_\eta = \frac{2\pi}{\eta}$  (as used in Pope, 2000). The ratio of the Dougherty-Ozmidov scale to Kolmogorov scale is  $\frac{L_O}{\eta} = 2\pi Re_b^{3/4}$ . So large  $Re_b$  ( $Re_b \gg 1$  Brethouwer et al., 2007) is required for the separation between  $L_O$  and  $\eta$ . The Dougherty-Ozmidov scale is of the order of meters (Jiménez & Cuxart, 2005; Li et al., 2016), while the Kolmogorov scale is of the order of millimeters in the ABL (Bradley et al., 1981; Gulitski et al., 2007). In the rest of this manuscript we thus assume that both conditions  $Fr_h \ll 1$  and  $Re_b \gg 1$  are met.

## 2.2. Approximation of Stratification Effects

We start from the spectral TKE balance equation (Lumley & Panofsky, 1964) following Weinstock (1978),

$$\frac{\partial E(k)}{\partial t} + \frac{\partial Q(k)}{\partial z} = S(k) \frac{\partial U_0}{\partial z} - \frac{\partial \epsilon(k)}{\partial k} + B(k) - 2\nu k^2 E(k), \quad (3)$$

where  $E(k)$  is spectral kinetic energy density,  $\frac{\partial Q(k)}{\partial z}$  is the vertical transfer of turbulent energy in physical space,  $S(k)$  is the cospectrum of the Reynolds stress  $-\overline{u'w'}$ ,  $u'$  and  $w'$  are streamwise and vertical velocity fluctuations, respectively,  $U_0$  is mean streamwise velocity,  $\epsilon(k)$  is net rate of spectral energy transfer,  $B(k)$  is the cospectrum of buoyancy flux  $-\frac{g}{\rho_0} \overline{w'\rho'}$ ,  $g$  is the gravitational acceleration rate,  $\rho_0$  is the mean density of air and  $\rho'$  the fluctuation, and  $2\nu k^2 E(k)$  is rate of energy dissipation by molecular viscosity  $\nu$ . Assuming steady state, neglecting  $\frac{\partial Q(k)}{\partial z}$  for eddies smaller than the energy-containing scales as in other literature (Dalaudier & Sidi, 1990; Lumley, 1964; Monin & Yaglom, 1975; Phillips, 1965; Sidi & Dalaudier, 1989) and neglecting molecular viscosity (i.e., for eddies much larger than the Kolmogorov scale), Weinstock (1978) obtained

$$\frac{\partial \epsilon(k)}{\partial k} = S(k) \frac{\partial U_0}{\partial z} + B(k), \quad (4)$$

for the equilibrium range. The buoyancy flux cospectrum can also be written as  $B(k) = -R_f S(k) \frac{\partial U_0}{\partial z}$  (Lumley, 1965), where  $R_f = \frac{g}{\theta_0} \frac{\overline{w'\theta'}}{\overline{u'w'} \frac{\partial U_0}{\partial z}}$  is the flux Richardson number and  $\theta'$  is fluctuation from the mean potential temperature  $\theta_0$ . Substituting  $B(k)$  into the spectral balance equation, Weinstock (1978) obtained

$$\frac{\partial \epsilon(k)}{\partial k} = B(k) \left( 1 - \frac{1}{R_f} \right), \quad (5)$$

where  $R_f > 0$  for stratified turbulence. Note that equation (5) applies to any scalar wavenumber for steady-state turbulence in the equilibrium range. Weinstock did not realize that there is an upper bound (Nieuwstadt, 1984; Schumann & Gerz, 1995; Townsend, 1958; Zilitinkevich et al., 2013) for  $R_f$  under steady-state assumption. Here we will take the upper bound of  $R_f$  to be 0.25 (Katul et al., 2014; Nieuwstadt, 1984; Zilitinkevich et al., 2013) for the existence of continuous turbulence with Richardson-Kolmogorov cascade, which is discussed in detail in Grachev et al. (2013). Further calculations of  $B(k)$  in Weinstock (1978) (see details in the supporting information; Lumley, 1964; Weinstock, 1976) require a prior knowledge of the vertical velocity spectrum  $\langle w^*(\mathbf{k}, 0)w(\mathbf{k}, 0) \rangle$ . Weinstock (1978) assumed that stratified turbulence is “approximately isotropic” and hypothesized the following vertical velocity spectrum:

$$\langle w^*(\mathbf{k}, 0)w(\mathbf{k}, 0) \rangle = a \left( 1 - \frac{k_3^2}{k^2} \right) \frac{2\pi^2 E(k)}{k^2}, \quad (6)$$

where “ $a$ ” is the anisotropy factor given by

$$a = \begin{cases} 1, & k \geq k_{BW}, \\ 0.5, & k < k_{BW}. \end{cases} \quad (7)$$

$E(k)$  is the energy spectrum for scalar wavenumber and  $k_{BW}$  is a transition wavenumber defined later. Equation (6) assumed that turbulence is “approximately isotropic”; that is,  $w$  spectrum is at least half of  $u$  spectrum in isotropic turbulence. In the ABL, the existence of a wall and stratification can cause the  $w$  spectrum to deviate from the  $u$  spectrum at low horizontal wavenumbers ( $k_1$ ). Field observation (Grachev et al., 2013) and models (Katul et al., 2014) suggest a shallower slope than  $-5/3$  at low horizontal wavenumbers in  $w$  spectrum. To include the wall bounding effects, we follow Townsend (1976) and Katul et al. (2014) and consider the wavenumber  $k_a$  that satisfies

$$k_a z = 1, \quad (8)$$

where  $z$  is height above ground. We relax the “approximately isotropic” hypothesis and redefine the anisotropy factor “ $a$ ” as follows:

$$a = \begin{cases} 1, & k \geq \max(k_a, k_O), \\ \left(\frac{k}{\max(k_a, k_O)}\right)^{2/3}, & k < \max(k_a, k_O). \end{cases} \quad (9)$$

The anisotropy factor “ $a$ ” is related to the ratio of  $w$  spectrum to  $u$  spectrum. When  $k < \max(k_a, k_O)$ , “ $a$ ” decreases as  $k$  decreases ( $a \propto k^{2/3}$ ). Under this assumption, the  $w$  spectrum will have a slope shallower than  $-5/3$  (Grachev et al., 2013; Katul et al., 2014) at  $k < \max(k_O, k_a)$ , and the  $w$  variance will be smaller than the  $u$  variance as  $k$  decreases. As we show later in this section, different forms of the anisotropic factor  $a$  would not affect the spectral scaling in the buoyancy subrange and the isotropic inertial subrange if the changing trend of equation (9) with wavenumber  $k$  is preserved.

The buoyancy flux in the horizontal wavenumber  $k_1$  then has the following form by approximation (Weinstock, 1978):

$$B(k_1) = -N^2 E(k_1) \frac{ak_1 v_m}{0.8N^2 + k_1^2 v_m^2}, \quad (10)$$

where  $v_m$  is the root-mean-square of fluctuating velocity for eddies smaller than energy-containing range given as  $v_m^2 = \frac{2}{3} \int_{k_m}^{\infty} E(k_1) dk_1$  and  $k_m$  is the smallest wavenumber in the equilibrium range. Note that the approximation in equation (10) implies a nonlinear relation between  $N^2$  and  $B(k_1)$ , which is different from the linear relation in  $B(k_1) \propto -N^2 \epsilon(k_1)^{1/3} k_1^{-7/3}$  proposed by Lumley (1964). When  $0.8N^2 = k_1^2 v_m^2$ , a transition wavenumber can be defined as (Weinstock, 1978)

$$k_{BW} = \frac{0.8^{1/2} N}{v_m}, \quad (11)$$

which corresponds to the length scale  $L_{BW} = \frac{2\pi}{k_{BW}}$ . When  $0.8N^2 \gg k_1^2 v_m^2$ , the effect of buoyancy is large and  $B(k_1)$  is in the buoyancy subrange. Waite (2011) showed that the strongly stratified turbulence cascade breaks down at  $L_b$ , thus  $L_b$  might delimit the boundaries of strong and weak stratification effects. Augier et al. (2015) further suggested that scales between  $L_b$  and  $L_O$  are not in the strongly stratified turbulent range. If the wavenumber  $k_b$  satisfies the condition  $0.8N^2 \gg k_1^2 v_m^2$ , or equivalently

$$L_b \gg L_{BW}, \quad (12)$$

this would require  $1.118 \frac{v_m}{U} \ll 1$ . The condition  $1.118 \frac{v_m}{U} \ll 1$  implies that the wind fluctuation is not too strong compared to the mean wind (as the mean velocity is of the same order as root mean square velocity). When  $0.8N^2 \ll k_1^2 v_m^2$ , the effect of buoyancy is small and  $B(k_1)$  is in the inertial subrange. If the wavenumber  $k_O$  satisfies the condition  $0.8N^2 \leq k_1^2 v_m^2$ , or equivalently

$$L_O \leq L_{BW}, \quad (13)$$

this would require  $1.118 \frac{v_m}{U} \geq Fr_h^{\frac{1}{2}}$ . When the definition of  $Fr_h$  is interpolated, the condition  $1.118 \frac{v_m}{U} \geq Fr_h^{\frac{1}{2}}$  is equivalent to  $1.25N \geq \frac{\epsilon}{v_m^2}$ , which actually constrains the lower limit of stratification and is not a condition for weak stratification. We expect that at wavenumbers  $k_1 \gg k_O$  (Dougherty, 1961; Gargett et al., 1984;

Ozmidov, 1965), the effect of buoyancy can be neglected. In order to observe a transition region between the Dougherty-Ozmidov scale  $L_O$  and buoyancy scale  $L_b$ , we thus need to satisfy the condition:

$$Fr_h^{\frac{1}{2}} \leq 1.118 \frac{v_m}{U} \ll 1. \quad (14)$$

In horizontal wavenumber  $k_1$  of the equilibrium range in the stably stratified turbulence without wall effects, scales above  $L_b$  will thus be in the buoyancy subrange, scales much smaller than  $L_O$  will be in the isotropic inertial subrange, and scales in between will be in a transition region.

### 2.3. $E(k_1)$ of Isotropic Turbulence

Now we need to determine  $E(k_1)$  as a function of horizontal wavenumber  $k_1$  in equation (10). According to previous studies (Gargett et al., 1984; Grachev et al., 2015; Katul et al., 2014; Lang & Waite, 2019; Li et al., 2016; Townsend, 1976; Waite, 2011), we assume that  $E(k_1)$  follows the  $-5/3$  scaling of isotropic turbulence (Kolmogorov, 1941) at  $\max(k_O, k_a) \leq k_1 \ll k_\eta$ :

$$E(k_1) \propto \epsilon_0^{2/3} k_1^{-5/3}, \quad (15)$$

where  $\epsilon_0$  is the TKE dissipation rate.

### 2.4. $E(k_1)$ of Anisotropic Turbulence

Here we focus on anisotropic turbulence at  $k_1 < \max(k_O, k_a)$ . For strongly stratified turbulence, the horizontal length scale  $L_h$  is much larger than the vertical length scale  $L_v$  (Billant & Chomaz, 2001). Due to this anisotropy, we assume that  $E(k_1)$  is mainly related to the horizontal scale  $L_h$ , which is also a key hypothesis applied in Lindborg (2006). Dimensional analysis suggests that  $E(k_1) \sim u_{L_h}^2 L_h$ , where  $u_{L_h}$  is the fluctuating velocity scale corresponding to  $L_h$ . We further assume that  $E(k_1)$  is related to  $k_1$  and  $\eta$ . Therefore, we have the following form of  $E(k_1)$ , written in a similar way to the spectrum given in page 232 of Pope (2000),

$$E(k_1) = C_1 u_{L_h}^2 L_h f_{L_h}(k_1 L_h) f_\eta(k_1 \eta), \quad (16)$$

where  $C_1$  is a proportionality constant and  $f_{L_h}$  and  $f_\eta$  are specified independent nondimensional functions. Following Taylor's estimate (Taylor, 1935) that has been discussed in literature (McComb et al., 2010; Sreenivasan, 1984), we have

$$L_h = \frac{u_{L_h}^3}{\epsilon_{L_h}}, \quad (17)$$

where  $\epsilon_{L_h}$  is the energy transfer rate for eddies of length scale  $L_h$ . Combining the above equations, we have

$$E(k_1) = C_1 \epsilon_{L_h}^{2/3} L_h^{5/3} f_{L_h}(k_1 L_h) f_\eta(k_1 \eta). \quad (18)$$

In the equilibrium range where  $\frac{2\pi}{L_h} \ll k_1 < \max(k_O, k_a)$ , we assume that  $E(k_1)$  is independent of  $L_h$  and  $\eta$ , thus leading to

$$E(k_1) = C_1 \epsilon(k_1)^{2/3} L_h^{5/3} f_{L_h}(k_1) f_\eta(k_1) = C_1 \epsilon(k_1)^{2/3} f(k_1), \quad (19)$$

where  $\epsilon(k_1)$  is the spectral energy transfer rate dependent on wavenumber  $k_1$  and  $f(k_1) \equiv f_{L_h}(k_1) f_\eta(k_1)$ . Dimensional analysis suggests that  $f(k_1) \sim k_1^{-5/3}$ , which then leads to

$$E(k_1) = C_1 \epsilon(k_1)^{2/3} k_1^{-5/3}. \quad (20)$$

It is worth noting that the above dimensional analysis has also been applied in the spectral scaling of anisotropic turbulence in Lindborg (2006), where a  $k_h^{-5/3}$  was obtained for anisotropic turbulence and  $k_h$  is the horizontal wavenumber. Therefore, equation (20) is essentially for anisotropic turbulence and differs from the isotropic turbulence scaling of equation (15).

Considering the similar functional form of equations (20) and (15), for simplicity, we approximate both isotropic and anisotropic turbulence in the equilibrium range with the following equation:

$$E(k_1) = \begin{cases} C_0 \epsilon(k_1)^{2/3} k_1^{-5/3}, & \max(k_a, k_O) \leq k_1 \ll k_\eta, \\ C_1 \epsilon(k_1)^{2/3} k_1^{-5/3}, & \frac{2\pi}{L_h} \ll k_1 < \max(k_a, k_O), \end{cases} \quad (21)$$

where  $C_0 = 1.5$  (Sreenivasan, 1995),  $C_1$  is a constant to be determined, and the condition  $\epsilon(k_1) = \epsilon_0$  is satisfied at  $k_1 \geq \max(k_a, k_o)$ . There might be discontinuities at  $k_1 = \max(k_a, k_o)$ , but the above expression could avoid further assumptions. Note that we here only consider spectra of horizontal wavenumber ( $k_1$ ) in the ABL and that turbulence in the vertical direction ( $k_3$ ) is not homogeneous (Fiedler & Panofsky, 1970). Substituting the above equation into equation (10), we have

$$B(k_1) = \begin{cases} -C_0 N^2 \epsilon(k_1)^{\frac{2}{3}} \frac{v_m a k_1^{-2/3}}{0.8N^2 + k_1^2 v_m^2}, & k \geq \max(k_a, k_o), \\ -C_1 N^2 \epsilon(k_1)^{\frac{2}{3}} \frac{v_m a k_1^{-2/3}}{0.8N^2 + k_1^2 v_m^2}, & k < \max(k_a, k_o). \end{cases} \quad (22)$$

As equation (5) holds for any scalar wavenumber for steady-state turbulence in the equilibrium range, we apply it to the horizontal wavenumber  $k_1$ , leading to

$$\frac{\partial \epsilon(k_1)}{\partial k_1} = B(k_1) \left(1 - \frac{1}{R_f}\right). \quad (23)$$

Combining the above two equations, we obtain

$$\frac{\partial \epsilon(k_1)}{\partial k_1} = \begin{cases} -C_0 N^2 \frac{v_m \epsilon(k_1)^{2/3} a k_1^{-2/3}}{0.8N^2 + k_1^2 v_m^2} \left(1 - \frac{1}{R_f}\right), & k_1 \geq \max(k_a, k_o), \\ -C_1 N^2 \frac{v_m \epsilon(k_1)^{2/3} a k_1^{-2/3}}{0.8N^2 + k_1^2 v_m^2} \left(1 - \frac{1}{R_f}\right), & k_1 < \max(k_a, k_o). \end{cases} \quad (24)$$

Solving the above equation, we have a similar form as Weinstock (1978):

$$[\epsilon(k_1)]^{1/3} = \begin{cases} \epsilon_0^{1/3} - \left(\frac{C_0 N^2 v_m}{3}\right) \int_{\infty}^{k_1} dk \frac{a k^{-2/3}}{0.8N^2 + k^2 v_m^2} \left(1 - \frac{1}{R_f}\right), & k_1 \geq \max(k_a, k_o), \\ \epsilon_0^{1/3} - \left(\frac{C_0 N^2 v_m}{3}\right) \int_{\infty}^{\max(k_a, k_o)} dk \frac{a k^{-2/3}}{0.8N^2 + k^2 v_m^2} \left(1 - \frac{1}{R_f}\right) - \left(\frac{C_1 N^2 v_m}{3}\right) \int_{\max(k_a, k_o)}^{k_1} dk \frac{a k^{-2/3}}{0.8N^2 + k^2 v_m^2} \left(1 - \frac{1}{R_f}\right), & k_1 < \max(k_a, k_o). \end{cases} \quad (25)$$

where  $\epsilon(k_1) \rightarrow \epsilon_0$  as  $k_1 \rightarrow \infty$ . The integral in the above equation can be written as

$$- \int_{\infty}^{k_1} dk \frac{a k^{-2/3}}{0.8N^2 + k^2 v_m^2} = \frac{k_{BW}^{-5/3}}{v_m^2} C \left(\frac{k_1}{k_{BW}}\right). \quad (26)$$

Equation (25) then reduces to

$$[\epsilon(k_1)]^{1/3} = \epsilon_0^{1/3} \left[1 + \frac{C_0 N^2}{3 \epsilon_0^{1/3} k_{BW}^{5/3} v_m} C \left(\frac{k_1}{k_{BW}}\right) \left(1 - \frac{1}{R_f}\right)\right]. \quad (27)$$

Substituting  $0.8N^2 = k_{BW}^2 v_m^2$  into the above equation, we have

$$[\epsilon(k_1)]^{1/3} = \epsilon_0^{1/3} \left[1 + \frac{5C_0^{3/2}}{12} \frac{v_m}{v_0} C \left(\frac{k_1}{k_{BW}}\right) \left(1 - \frac{1}{R_f}\right)\right], \quad (28)$$

where  $v_0^2 = \frac{2}{3} \int_{k_{BW}}^{\infty} E(k_1) dk_1$  (Weinstock, 1978). Combining with equation (20), we have the following  $E(k_1)$  for the equilibrium range at  $\frac{2\pi}{L_h} \ll k_1 \ll k_\eta$ :

$$E(k_1) = C_0 \epsilon_0^{\frac{2}{3}} \left[1 - \frac{5C_0^{3/2}}{12} \frac{v_m}{v_0} \left(\frac{1 - R_f}{R_f}\right) C \left(\frac{k_1}{k_{BW}}\right)\right]^2 k_1^{-\frac{5}{3}}. \quad (29)$$

Note that the above equation will have to recover equation (15) for isotropic turbulence at  $k_1 \geq \max(k_o, k_a)$ . As  $Fr_h \ll 1$  is assumed in this manuscript, the neutral limit  $R_f \rightarrow 0$  is not expected and the above equation does not blow up due to  $\frac{1-R_f}{R_f}$ . Details of the functional forms of  $C\left(\frac{k_1}{k_{BW}}\right)$  defined in equation (26) under different cases in the ABL are discussed as follows.

**2.4.1. Case  $k_a \leq k_O$**

If  $k_a \leq k_O$  (i.e.,  $L_O \leq 2\pi z$ ), similarly to Weinstock (1978), we obtain

$$C\left(\frac{k_1}{k_{BW}}\right) = \begin{cases} \frac{\frac{3}{5}\left(\frac{k_O}{k_{BW}}\right)^{-\frac{5}{3}}}{1+\frac{1}{5}\left(\frac{k_O}{k_{BW}}\right)^{-2}} + \frac{C_1}{C_0}\left(\frac{k_{BW}}{k_O}\right)^{\frac{2}{3}} \left[ \arctan\left(\frac{k_O}{k_{BW}}\right) - \arctan\left(\frac{k_1}{k_{BW}}\right) \right], & k_1 < k_O, \\ \frac{\frac{3}{5}\left(\frac{k_1}{k_{BW}}\right)^{-\frac{5}{3}}}{1+\frac{1}{5}\left(\frac{k_1}{k_{BW}}\right)^{-2}}, & k_1 \geq k_O. \end{cases} \quad (30)$$

In the limit of high wavenumbers, the above equation reduces to

$$\lim_{\frac{k_1}{k_{BW}} \rightarrow \infty} C\left(\frac{k_1}{k_{BW}}\right) = \lim_{\frac{k_1}{k_{BW}} \rightarrow \infty} \frac{\frac{3}{5}\left(\frac{k_1}{k_{BW}}\right)^{-\frac{5}{3}}}{1+\frac{1}{5}\left(\frac{k_1}{k_{BW}}\right)^{-2}} = 0. \quad (31)$$

When  $k_1 \gg k_O$ , the condition  $Fr_h^{\frac{1}{2}} \leq 1.118 \frac{v_m}{U}$  ensures  $\frac{k_1}{k_{BW}} \gg 1$ , so that  $E(k_1) = C_0 \epsilon_0^{\frac{2}{3}} k_1^{-\frac{5}{3}}$  is a good approximation, and thus, the spectrum follows the  $-5/3$  scaling of isotropic turbulence. When  $k_1 < k_O$ , letting

$$A = \frac{5C_0^{\frac{3}{5}} v_m}{12 v_0} \left( \frac{1-R_f}{R_f} \right), \text{ we obtain}$$

$$\begin{aligned} \left[ 1 - AC\left(\frac{k_1}{k_{BW}}\right) \right]^2 &= \sigma_0^2 - 2An\sigma_0 \frac{k_1}{k_{BW}} + A^2 n^2 \left(\frac{k_1}{k_{BW}}\right)^2 + \frac{2}{3} An\sigma_0 \left(\frac{k_1}{k_{BW}}\right)^3 \\ &+ O\left(\left(\frac{k_1}{k_{BW}}\right)^4\right) > 0, \end{aligned} \quad (32)$$

where  $\sigma_0 = A \left( m + n \arctan\left(\frac{k_O}{k_{BW}}\right) \right) - 1$ ,  $m = \frac{\frac{3}{5}\left(\frac{k_O}{k_{BW}}\right)^{-\frac{5}{3}}}{1+\frac{1}{5}\left(\frac{k_O}{k_{BW}}\right)^{-2}}$ , and  $n = \frac{C_1}{C_0} k_{BW}^{\frac{2}{3}} k_O^{-\frac{2}{3}}$ . At  $k_b < k_1 < k_O$ , the spectral slope may vary at different stability conditions and we will refer to observations. For the largest eddies,  $k_1 < k_b$ , the condition  $1.118 \frac{v_m}{U} \ll 1$  ensures that  $\frac{k_1}{k_{BW}} \ll 1$ , so that  $E(k_1) = C_0 \epsilon_0^{\frac{2}{3}} \sigma_0^2 k_1^{-\frac{5}{3}}$  is a good approximation, and thus, we would expect the spectrum to exhibit a shape similar to the isotropic one but for different physical reasons. This also suggests that  $\epsilon(k_1)$  is independent of  $k_1$  at  $k_1 < k_b$ . Thus, equation (22) for  $B(k_1)$  together with equation (9) for the anisotropic factor “ $a$ ” would lead to the result that  $B(k_1)$  has a 0 slope at lowest  $k_1$ , which is consistent with approximations in literature (Horst, 1997; Kaimal, 1973; Kaimal et al., 1972; Massman, 2000; Massman & Lee, 2002). Note that the anisotropy factor  $a$  influences  $C\left(\frac{k_1}{k_{BW}}\right)$  in equation (26). However, the asymptotic value of equation (32) approaches a constant at  $k_1 < k_b$  as long as the anisotropy factor  $a$  decreases as  $k$  decreases in low wavenumbers, so that the spectral scaling at  $k_1 < k_b$  is not influenced. Besides, the spectral scaling at  $k_b < k_1 < k_O$  relies on observation, and the  $-5/3$  scaling is expected at  $k_1 \gg k_O$  due to isotropic turbulence. Then different forms of the anisotropic factor  $a$  would not affect the spectral scaling in the equilibrium range if the decreasing trend of  $a$  is similar to that of equation (9). Therefore, we expect  $E(k_1)$  spectra to exhibit a  $-5/3$  power law scaling both below  $k_b$  and above  $k_O$  and having a scaling that may be different from  $-5/3$  in the transition region between  $k_b$  and  $k_O$ .

**2.4.2. Case  $k_a > k_O$**

If  $k_a > k_O$  (i.e.,  $L_O > 2\pi z$ ), similarly to Weinstock (1978), we have

$$C\left(\frac{k_1}{k_{BW}}\right) = \begin{cases} \frac{\frac{3}{5}\left(\frac{k_a}{k_{BW}}\right)^{-\frac{5}{3}}}{1+\frac{1}{5}\left(\frac{k_a}{k_{BW}}\right)^{-2}} + \frac{C_1}{C_0}\left(\frac{k_{BW}}{k_a}\right)^{\frac{2}{3}} \left[ \arctan\left(\frac{k_a}{k_{BW}}\right) - \arctan\left(\frac{k_1}{k_{BW}}\right) \right], & k_1 < k_a, \\ \frac{\frac{3}{5}\left(\frac{k_1}{k_{BW}}\right)^{-\frac{5}{3}}}{1+\frac{1}{5}\left(\frac{k_1}{k_{BW}}\right)^{-2}}, & k_1 \geq k_a. \end{cases} \quad (33)$$

Analogously to section 2.4.1 with  $k_O$  replaced by  $k_a$ , we obtain the following results: At  $k_1 \gg k_a$ , the spectrum follows the  $-5/3$  scaling of isotropic turbulence; at  $k_b < k_1 < k_a$ , the spectral slope in this case is uncertain at different stability conditions; and at  $k_1 < k_b$ , the spectrum follows a  $-5/3$  scaling that has different physical reason compared to the isotropic turbulence.

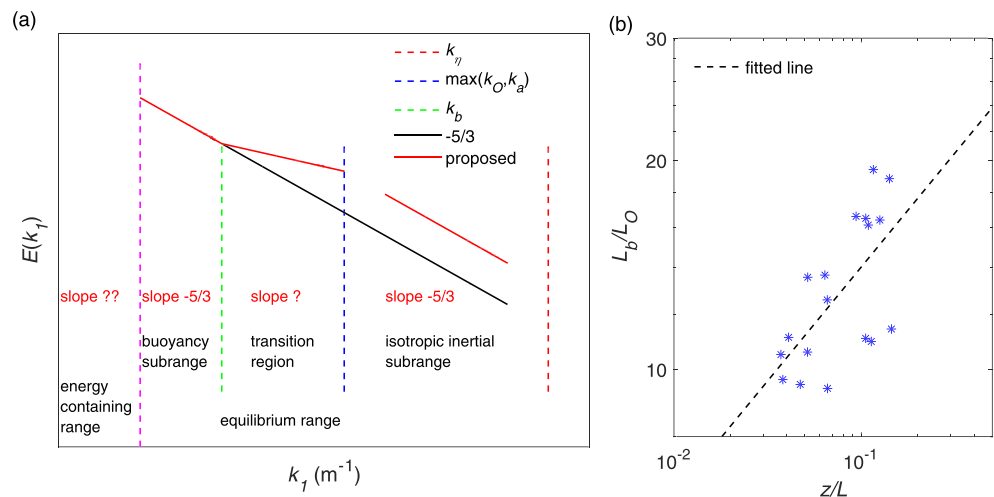


**Figure 1.** (a) Schematic of TKE (temperature) spectrum  $E(k_1)$  in horizontal wavenumber  $k_1$  in the stable atmospheric boundary layer. (b) The scatter plot between the ratio of the buoyancy scale  $L_b$  to the Dougherty-Ozmidov scale  $L_0$  and  $z/L$  of the lake EC data.  $z$  is measurement height above the surface, and  $L$  is the Obukhov length.

To summarize, the major hypotheses in this study that are different from Weinstock (1978) are equations (9), (10), and (21), where we do not assume that the  $k_1$  and  $k_3$  spectra are the same or that  $u$  and  $w$  spectra are similar for small  $k_1$  in the equilibrium range. Unlike Weinstock (1978) that treats turbulence as “approximately isotropic,” we have included a separate discussion of isotropic and anisotropic turbulence in  $k_1$  for the equilibrium range. Based on our findings, we expect the following three regions (schematic in Figure 1a) of turbulence spectra in horizontal wavenumber  $k_1$  of the equilibrium range in the stable ABL: the isotropic inertial subrange at  $k_1 \gg \max(k_O, k_a)$ ; the transition region at  $k_b < k_1 < \max(k_O, k_a)$ ; and the buoyancy subrange with the  $-5/3$  power law scaling at  $k_1 < k_b$ . How  $E(k_1)$  varies with the stratification factor  $Fr_h$  is introduced below. As  $Fr_h$  increases from strong stratification ( $Fr_h \rightarrow 0$  and  $L_0 \leq 2\pi z$ ) toward weaker stratification (i.e.,  $N$  decreases),  $L_0$  and  $L_b$  increase,  $\frac{L_b}{L_0} = Fr_h^{-1/2}$  decreases, and the transition region between  $L_0$  and  $L_b$  shrinks. When  $L_0 > 2\pi z$ , the transition region is denoted by  $L_b$  and  $z$ . A  $-5/3$  scaling is expected at scales larger than  $L_b$ , a shallower slope between  $L_b$  and  $z$ , and a  $-5/3$  scaling at the length scales much smaller than  $z$ . As  $Fr_h$  approaches or exceeds 1,  $L_0$  or  $L_b$  could even exceed the largest scale of the equilibrium range. The spectrum in the equilibrium range will consist of two regions: a  $-5/3$  scaling at the length scales much smaller than  $z$  and a shallower scaling at the length scales larger than  $z$ . Besides, we assume that the potential temperature spectrum  $E_\theta(k_1)$  has similar three regions as  $E(k_1)$  in the stable ABL, since their similar spectral slopes have been reported (Kaimal, 1973; Kaimal et al., 1972; Smedman, 1988). To confirm our theoretical approximation, we now turn to results from field observations and DNS.

### 3. Field Observations and Numerical Results

#### 3.1. Observations of the Stable ABL

High-frequency (20 Hz) velocity and temperature were recorded at four different heights (1.66, 2.31, 2.96, and 3.61 m above the water surface) with eddy covariance (EC) systems in the stable ABL over Lake Geneva during August–October 2006 (Bou-Zeid et al., 2008). Wind velocity measurements had errors (mean velocity deviation from the truth) on the order of 0.021 m/s with a maximum of 0.054 m/s under zero wind conditions (Vercauteren et al., 2008). Wind velocity had a standard derivation of 0.001 m/s from instruments. Mean temperature measurements were corrected by the relative mean offsets of instruments. The instruments had a standard deviation of 0.002° for temperature measurements. Eighteen periods of 15 min in the stable ABL were selected (Table 1). The mean of  $1.118 \frac{v_m}{U} / Fr_h^{1/2}$  in the selected 18 periods was 1.22, and the mean of  $1.118 \frac{v_m}{U}$  was 0.087, thus satisfying equation (14). The Kolmogorov scales ( $\eta$ ) in these periods were of the order of 0.001 m. Details of the experiment setup and data can be found in Bou-Zeid et al. (2008), Vercauteren et al. (2008), Li and Bou-Zeid (2011), and Li et al. (2018).

High-frequency (10 Hz) velocity and temperature were recorded at 3.5 m above ground with EC in Dome C, Antarctica (Vignon, Genthon, et al., 2017; Vignon, van de Wiel, et al., 2017). The temperature gradient



**Table 1**

*Details of Selected Stable Periods in Field Observations: Eddy Covariance (EC) Systems Over Lake Geneva, EC Systems at Dome C in Antarctica, and Distributed Temperature Sensing (DTS) Systems in Oklahoma*

Data source	# of periods	$u_*$ (m/s)	$T_*$ (K)	$z/L$	$R_f$	$Fr_h$
Lake Geneva	18	0.07–0.17	0.02–0.10	0.037–0.145	0.03–0.09	0.003–0.011
Dome C	60	0.03–0.13	0.02–0.15	0.409–5.891	0.14–0.21	—
DTS	2	0.02–0.04	0.02–0.09	1.236–2.398	0.18–0.20	—

*Note.*  $u_*$  is the friction velocity,  $T_*$  is the scaling temperature,  $z$  is measurement height above the surface,  $L$  is the Obukhov length,  $R_f$  is the flux Richardson number, and  $Fr_h$  is the horizontal Froude number.

in the stable ABL was obtained from balloon sounding measurements (Petenko et al., 2019). Sixty periods of 30-min observation in the stable ABL from 9 to 12 January 2015 were selected (Table 1). The mean of  $1.118 \frac{v_m}{U}$  in the selected 60 periods was 0.057, thus satisfying equation (14). Wind speed measurements had an accuracy of 0.05 m/s, and temperature had an accuracy of  $0.01^\circ$  (Vignon, Genthon, et al., 2017). Details of the EC setup and the site can be found in Vignon et al. (2017).

Fiber optics were set up at four heights (1.00, 1.25, 1.50, and 1.75 m above ground) along a 233-m-long transect at Oklahoma State University Range Research Station from 20 May to 15 July 2016. Details of the distributed temperature sensing (DTS) (Selker et al., 2006; Tyler et al., 2009) experiment can be found in Cheng et al. (2017). Temperature data were collected every 0.127 m along the fiber and every 1.5 s. Mean wind velocity  $U$  and scaling temperature  $T_* = -\frac{wT'}{u_*}$  ( $u_*$  is the friction velocity) were obtained from a nearby EC tower. Two representative 30-min periods in the stable nocturnal boundary layer were analyzed (Table 1). Temperature resolution were  $0.16^\circ$  and  $0.22^\circ$  before and after the fiber optics transect, respectively. The effective spatial resolution was 0.56 m, and temporal resolution was 3 s.

White Gaussian noise in instruments will typically cause a flat spectrum, so high-wavenumber spectrum will be influenced more by instrumental noise. In one subplot of the TKE spectra (Figure 2) and one subplot of temperature spectra (Figure 4) in the Lake EC data, a shallower slope than  $-5/3$  can be seen at the highest wavenumbers, which indicates the influence of instrumental white Gaussian noise. In the spectra plots of the Dome C data, though the influence of white noise is not obvious. In temporal spectra of DTS data, the measured temperature variation inside the cooler box with constant temperature is regarded as white Gaussian noise, which is then removed from the raw temperature spectra (Schilperoort, personal communication, December 15, 2017).

### 3.2. DNS of Stably Stratified Ekman Layer

DNS has recently been applied to study atmospheric turbulence under both unstable and stable conditions despite the known caveat of being at a much lower Reynolds number than the real atmosphere (Anson & Mellado, 2014; Chung & Matheou, 2012; Gohari & Sarkar, 2017; Li et al., 2018; Mellado et al., 2016; Shah & Bou-Zeid, 2014). It has also been shown by previous studies that LES may have difficulties predicting strongly stable flows (He & Basu, 2015; Jiménez & Cuxart, 2005). Therefore, to closely examine the spectral scaling proposed in the previous section, we simulated a stable Ekman layer flow.

The incompressible Navier-Stokes equations with Boussinesq approximation and the temperature equation are numerically integrated in time. The flow is driven by a steady pressure gradient, assuming a geostrophic balance in regions far above the surface, where the Coriolis force balances the large-scale pressure gradient. Numerical details of the code can be found in Shah and Bou-Zeid (2014) and Li et al. (2018). A neutrally stratified turbulent Ekman layer flow (Coleman et al., 1992) over a smooth surface is first simulated for  $ft = 3$  with  $Re_D = U_g D/\nu$ , where  $f$  is the Coriolis parameter,  $t$  is time,  $U_g$  is the geostrophic wind speed,  $D = \sqrt{2\nu/f}$  is the laminar Ekman layer depth, and  $\nu$  is the viscosity of air. The mean velocity in wall units fits the expected log-law for the first  $ft = 3$  neutrally stratified flow, which has also been obtained in the neutral Ekman layer simulations in Shah and Bou-Zeid (2014) and Gohari and Sarkar (2017). A cooling surface buoyancy flux  $B_0$ , constant in time (i.e., a Neumann boundary condition), is then applied, similarly to Gohari and Sarkar (2017). In the DNS simulation,  $Fr_h = 0.0011$  and  $Re_b = 7.1$ ; thus, the assumption of small  $Fr_h$  is satisfied and the assumption for  $Re_b$  marginally applies in the analyses of section 2. We impose a zero heat flux condition as the top boundary and apply damping in a sponge layer at the top 25% of the computation domain to prevent reflection of gravity waves.

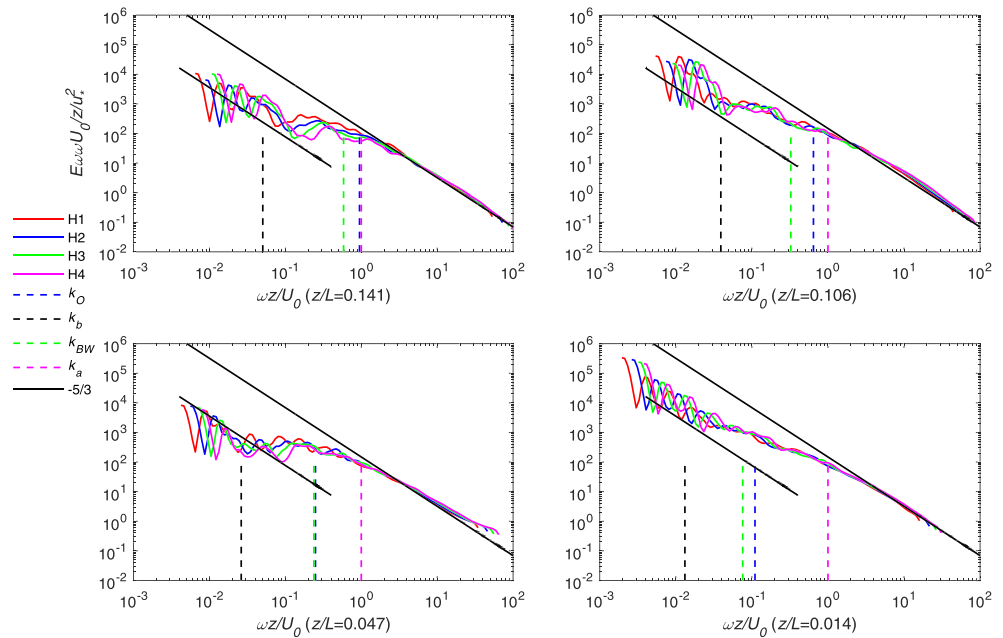


**Figure 2.** Normalized temporal wavelet spectra of TKE in four representative 15-min periods of the EC data over Lake Geneva.  $E_{\omega\omega}$  is wavelet spectrum in frequency,  $U_0$  is mean streamwise wind velocity,  $z$  is measurement height above lake,  $u_*$  is the friction velocity,  $\omega = 2\pi f$  is angular frequency, and  $L$  is the Obukhov length. “H1,” “H2,” “H3,” and “H4” denote observation heights 1.66, 2.31, 2.96, and 3.61 m above the lake, respectively. “ $k_O$ ,” “ $k_b$ ,” “ $k_{BW}$ ,” and “ $k_a$ ” are the wavenumber corresponding to the Dougherty-Ozmidov scale, the buoyancy scale,  $L_{BW}$ , and the distance to the wall, respectively.

A stably stratified Ekman flow is often used to represent an idealized stable planetary boundary layer (Anson & Mellado, 2014). The bulk Richardson number  $Ri_B = \frac{g\delta_*}{U_g^2} \frac{\theta_{ref} - \theta_0}{\theta_{ref}}$  evolves with time, where  $\delta_*$  is the turbulent Ekman layer length scale given by  $\delta_* = u_*/f$ ,  $\theta_{ref}$  is the reference potential temperature at far distance and  $\theta_0$  is the surface temperature, which changes with time as a result of the imposed cooling buoyancy flux. We can use the Obukhov length scale  $L$  (Obukhov, 1946) to measure the near-surface stability, which is then scaled with the inner variables to obtain  $L^+ = -\frac{u_*^3}{\kappa g \overline{w'\theta'}} \frac{u_*}{v}$ , where  $\kappa$  is the von Kármán constant,  $g$  is the

gravitational constant  $9.81 \text{ m/s}^2$ ,  $\frac{g}{\theta_0} \overline{w'\theta'}$  is the surface buoyancy flux  $B_0$ , and  $u_* = \left[ \left( v \frac{\partial u}{\partial z} \Big|_0 \right)^2 + \left( v \frac{\partial v}{\partial z} \Big|_0 \right)^2 \right]^{1/4}$ . Using  $u_*$  computed from the neutrally stratified case before  $B_0$  is applied, we define the initial  $L^+(t=0)$  as a measure of the strength of stratification. At  $t=0$  (i.e., after the neutral Ekman layer is simulated for  $ft=3$ , which is sufficient to obtain a distinct region that follows the logarithmic law similar to Shah & Bou-Zeid, 2014; Gohari & Sarkar, 2017), the surface buoyancy flux  $B_0$  is imposed.  $u_*/U_g$  for the neutrally stratified Ekman flow is 0.05370, which compares favorably with studies in the literature (e.g.,  $u_*/U_g = 0.05350$  for  $Re = 1000$  in Spalart et al., 2008; see their Table 2).  $B_0$  is defined as  $\frac{u_*^3}{\kappa L(t=0)}$ , where  $L(t=0) = \frac{v}{u_*} L^+(t=0)$ .  $L^+(t=0) = 1,600$  determines the magnitude of the buoyancy flux applied and stability strength measured by  $L^+$  changes with time. The stability strength can also be understood from the ratio of turbulent Ekman layer depth  $\delta_*$  to  $L(t)$ . For example,  $\frac{L(t=0.2/f)}{\delta_*} \approx 0.6$  is considered stably stratified (Gohari & Sarkar, 2017). Table 2 shows more details of the setup. Note that dimensionless numbers  $Re_D$  and  $L^+$  are sufficient to completely specify the dynamics of Ekman layer flows considered in this study. The buoyancy scale is computed from DNS as  $L_b = 2\pi U/N$ , where  $U$  is root-mean-square of the horizontal velocity,  $N$  is computed from the local vertical temperature gradient, and  $g$  is the acceleration of gravity.

### 3.3. Turbulence Spectra in Horizontal Wavenumber

The stability of the atmosphere can also be characterized by  $z/L$ , where  $z$  is the measurement height above the surface,  $L = -\frac{u_*^3}{\kappa g \overline{w'\theta'}}$  is the Obukhov length (Monin & Obukhov, 1954; Obukhov, 1946),  $u_*$  is the friction velocity, and  $\theta'$  the fluctuation from mean potential temperature  $\theta_0$ . Note that we use air temperature to approximate the potential temperature as our field observations were very close to the surface. Frequency

**Table 2**

Details of DNS Setup

$Re_D$	$L^+(t=0)$	$L_x, L_y, L_z$	$\Delta x(y)^+, \Delta z^+$	$N_x \times N_y \times N_z$
1,000	1,600	90D, 90D, 30D	3.90, 0.353	$1,024 \times 1,024 \times 3,840$

Note.  $L_x, L_y,$  and  $L_z$  are the dimensions of computational domain in  $x$  (streamwise),  $y$  (spanwise), and  $z$  (vertical) directions, respectively;  $\Delta x(y)^+, \Delta z^+$  are the resolutions in  $x(y)$  and  $z$  directions;  $N(x, y, z)$  denotes the number of points for computation;  $D = \sqrt{2\nu/f}$  is the laminar Ekman layer depth;  $L^+$  is the normalized Obukhov length. Note that we have used uniform grid spacing and  $L_x, L_y,$  and  $L_z$  in wall units (i.e.,  $L_{x,(y,z)}u_* / \nu$ ) are 3,994, 3,994, and 1,355, respectively.

spectra were transformed into  $k_1$  spectra invoking Taylor’s frozen turbulence hypothesis (Taylor, 1938). Wavelet spectra (Torrence & Compo, 1998) of temporal series (the wavelet software was provided by C. Torrence and G. Compo and is available at <http://paos.colorado.edu/research/wavelets/>) were calculated.

Similarly to Kaimal et al. (1972), both energy spectra (wavelet) in horizontal wavenumber  $k_1$  and frequency are normalized in log-log plots. In TKE spectra of Lake EC (Figure 2) and Dome C data (Figure 5a), there are three regions corresponding to the buoyancy subrange, a transition region and the isotropic inertial subrange. At  $k_1 > \max(k_o, k_a)$ , the spectra match the  $-5/3$  power law scaling of isotropic turbulence. The observation also shows that the Dougherty-Ozmidov scale  $L_o$  is a better demarcation of the isotropic inertial subrange compared to  $L_{BW}$  defined in Weinstock (1978) (as we suggested in equation (13)). In the transition region at  $k_b < k_1 < \max(k_o, k_a)$ , the slope of spectra is not universal but less steep than  $-5/3$ . Katul et al. (2012) has reported a  $-1$  slope at low wavenumbers in the TKE spectra of the stable ABL. It appears to be a specific case of the transition region described here, with a slope not as steep as  $-5/3$ . Above the buoyancy scale, observations seem to show another  $-5/3$  slope, which agrees with the spectra shown in Figure 7 of Muschinski et al. (2004) and is consistent with the theoretical approximation presented in section 2.

To better identify the spectral slope of TKE, we used the compensated wavelet spectrum that multiplies the spectrum by  $f^{5/3}$  ( $f$  is sampling frequency in hertz). We selected the median spectrum of 18 different periods at each frequency in Lake EC data (Figure 3a) and the median spectrum of 60 periods at each frequency in Dome C data (Figure 6a). At high frequencies over 1 Hz, the premultiplied TKE spectrum approaches a flat slope in both the Lake and Dome C data, consistent with the  $-5/3$  scaling in isotropic inertial subrange. At frequencies between approximately 0.01 and 1 Hz, there is mainly a positive and varying slope (Figures 3a and 6a); that is, the slope is shallower than  $-5/3$  scaling in the transition region. At low frequencies below 0.01 Hz in the Lake data (Figure 3a), the compensated spectrum oscillates a lot but the overall

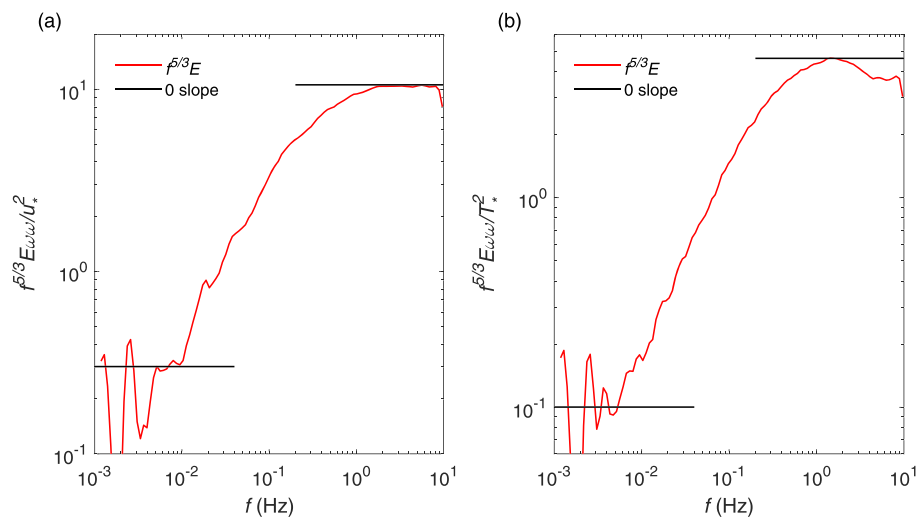


**Figure 3.** Median of compensated temporal wavelet spectra of (a) TKE and (b) temperature for each frequency in 18 representative 15-min periods of the Lake EC data.  $E_{\omega\omega}$  is wavelet spectrum in frequency,  $u_*$  is the friction velocity,  $T_*$  is the scaling temperature, and  $f$  is the sampling frequency.

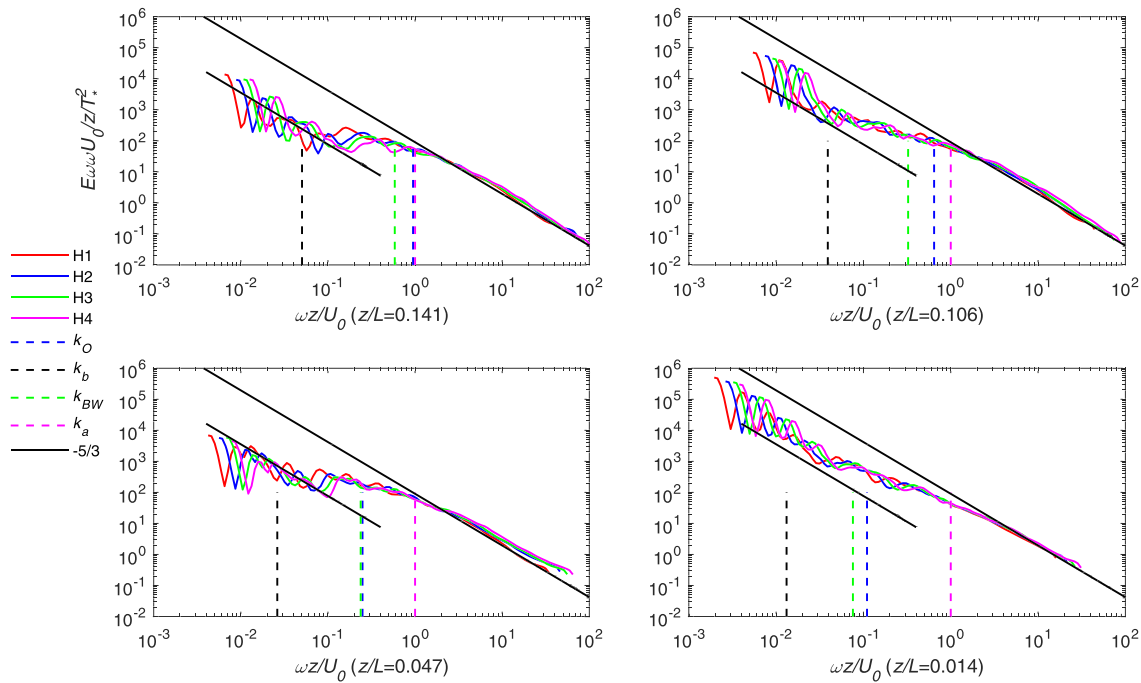


**Figure 4.** Temporal wavelet spectra of temperature in four representative 15-min periods of the Lake EC data.  $T_*$  is the scaling temperature, and other variables have the same meaning as those in Figure 2.

slope is shallower than the transition region. However, the Dome C data show a clear flat region between 0.004 and 0.01 Hz (Figure 6a), although the slope still varies across the wavenumber domain. The Dome C data ( $0.409 \leq z/L \leq 5.891$ ) are more stable than the Lake data ( $0.037 \leq z/L \leq 0.145$ ), thus having smaller buoyancy scales and larger buoyancy subrange. Also, the Dome C data have longer sampling periods (30 min) compared to the Lake data (15 min), leading to fewer oscillations at lowest frequencies in the former. Therefore, the compensated TKE spectrum of Dome C data (Figure 6a) better supports a  $-5/3$  slope in the buoyancy subrange and a shallower slope in the transition region.

In the temperature spectrum of the Lake (Figure 4) and Dome C data (Figure 5b) as well as compensated temperature spectrum (Figures 3b and 6b), three regimes similar to the TKE spectrum can be observed. We conjecture that the observed  $-1$  slope (Katul et al., 2016; Li et al., 2015) at low wavenumbers in the temperature spectra of the stable ABL might be a specific scaling in the transition region. In the temperature spectra of the DTS data (Figures 5c and 5d), only the buoyancy subrange and transition region are observed due to limited temporal and spatial resolution and temporal averaging (Cheng et al., 2017). The spatial spectra were used to check if the temporal spectra that invoke Taylor's frozen turbulence hypothesis (Taylor, 1938) are a good approximation, but those spatial spectra are more limited in terms of the number of decades they cover ( $\sim 3$ ). More detailed discussion on Taylor's hypothesis can be found in Cheng et al. (2017). Both temporal spectra and spatial spectra seem to exhibit an approximately  $-5/3$  slope at low wavenumbers and a shallower slope at high wavenumbers. The minimum length resolved in the temporal and spatial spectra were 4.00 and 1.52 m, respectively, which are close to the Dougherty-Ozmidov scale typically observed in the ABL (Jiménez & Cuxart, 2005; Li et al., 2016), so that we cannot observe the smaller-scale isotropic behavior. About one decade to the left of the Dougherty-Ozmidov scale, a  $-5/3$  scaling can be observed, corresponding to the buoyancy subrange previously defined. The transition region in the spatial spectra of DTS data has almost a 0 slope compared to the temporal spectra, which might be due to the influence of instrumental noise.

As the Reynolds number of the observed ABL is much higher than that of the DNS, some differences in turbulence spectra can be expected; for example, the inertial subrange is much narrower in the latter (Chung & Matheou, 2012; Shah & Bou-Zeid, 2014). The Kolmogorov scale  $\eta$  (see introduction in section 3.1) in the Lake EC data is about four decades away from the Dougherty-Ozmidov scale; that is, we observe a large

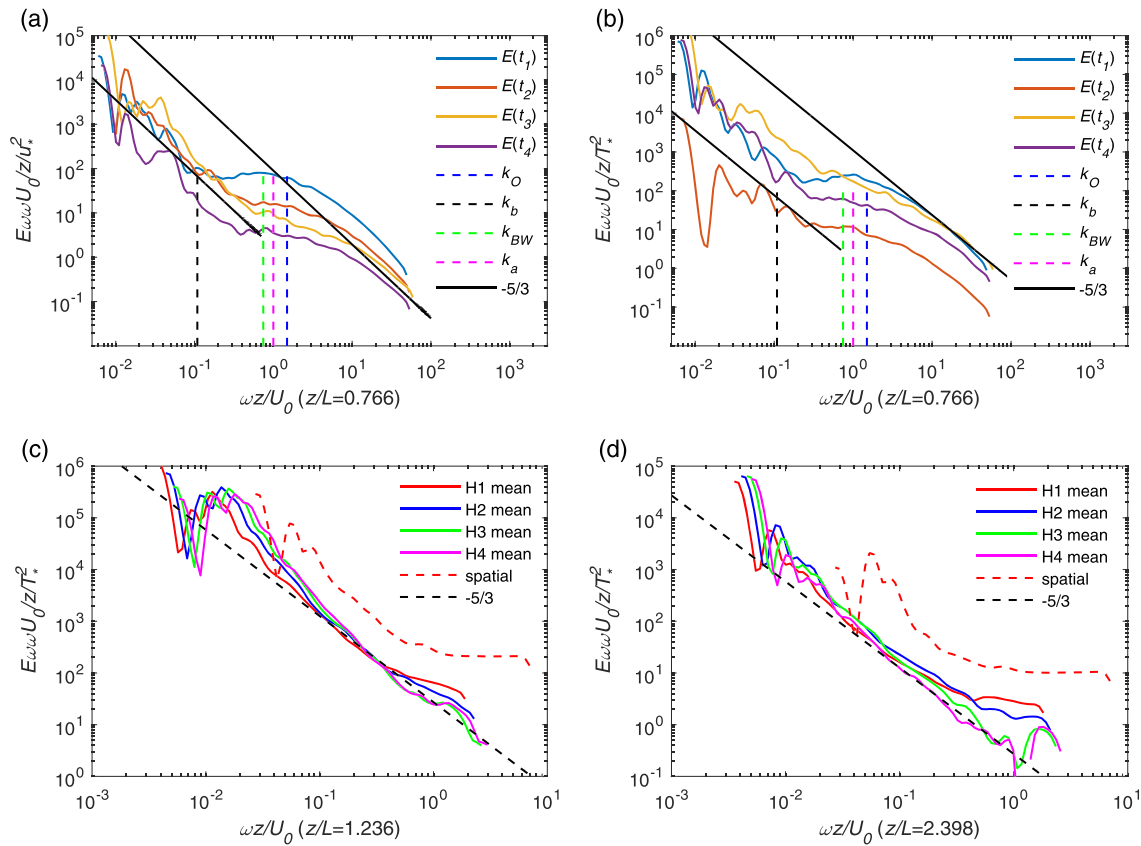


**Figure 5.** (a) Normalized temporal wavelet spectra of TKE in Dome C data. (b) Normalized temporal spectra of temperature in the Dome C data.  $T_s$  is scaling temperature, and other variables have the same meaning as those in Figure 1. “ $E(t_1)$ ,” “ $E(t_2)$ ,” “ $E(t_3)$ ,” and “ $E(t_4)$ ” denote the spectrum of four different 30-min stable periods on 9 January 2015 respectively.  $k_O$ ,  $k_b$ ,  $k_{BW}$ , and  $k_a$  denote wavenumbers in the time period of “ $E(t_1)$ .” (c and d) Spatial spectra and spatial mean of temporal spectra of temperature along fiber optics in two representative 30-min periods of DTS data. Only the buoyancy subrange and transition region are resolved due to limited temporal and spatial resolution and temporal averaging. Variables have the same meaning as those in Figure 2. “spatial” denotes the spatial spectra of temperature at height 1.75 m. “H1 mean,” “H2 mean,” “H3 mean,” and “H4 mean” denote the spatial mean of temporal spectra at four fiber optics measurement heights, respectively.

region of the isotropic inertial subrange, suggesting that turbulence is still well defined rather than being intermittent as shown in DNS results (Ansorge & Mellado, 2016; Flores & Riley, 2011).

In the DNS of stably stratified Ekman layer, the spectral bump (Figure 7) as  $Ri_B$  changes from 0.21, 0.65 to 0.98 in the DNS is not as clear as those shown in the atmospheric data. In the DNS,  $\frac{L_O}{\eta} = 4.3$  at  $z^+ = 65$ ; that is, the Dougherty-Ozmidov scale is very close to Kolmogorov scale (Waite, 2014). It may be argued that around the  $k_x z$  indicated by the scale of  $1/L_b$ , the spectral bump appears consistent with the scaling analysis above. However, because of computational limitations, current DNS can only achieve a narrow range of inertial subrange compared to the observational data in the stable ABL, which is at a much higher Reynolds number, and thus, current DNS does not appear to have sufficient scale separation (Kunkel & Marusic, 2006) to correctly represent the three regimes highlighted above due to the limitation of current computational capacity (Smyth & Moum, 2000). As stratification increases, the Dougherty-Ozmidov scale further decreases (and the wavenumber  $k_O$  increases), the spectra at highest wavenumbers become closer to the  $-5/3$  scaling and are less impacted by dissipative effects. However, a larger separation of scales between the inertial subrange and the dissipation range is required and not met with currently achievable DNS Reynolds numbers. In LES, the subgrid-scale filter size has to be smaller than the Dougherty-Ozmidov scale. The spectra below the Dougherty-Ozmidov scale are typically not resolved in LES (Beare et al., 2006; Khani & Waite, 2014; Waite, 2011) except possibly in a few studies (Sullivan et al., 2016).

A schematic of the TKE and temperature spectra in horizontal wavenumber  $k_1$  in the stable ABL is shown (Figure 1a). In the equilibrium range, the  $-5/3$  power law scaling at  $k_1 < k_b$  is due to stratification effects, while the  $-5/3$  scaling at  $k_1 \gg \max(k_O, k_a)$  is due to isotropic turbulence. In the intermediate transition

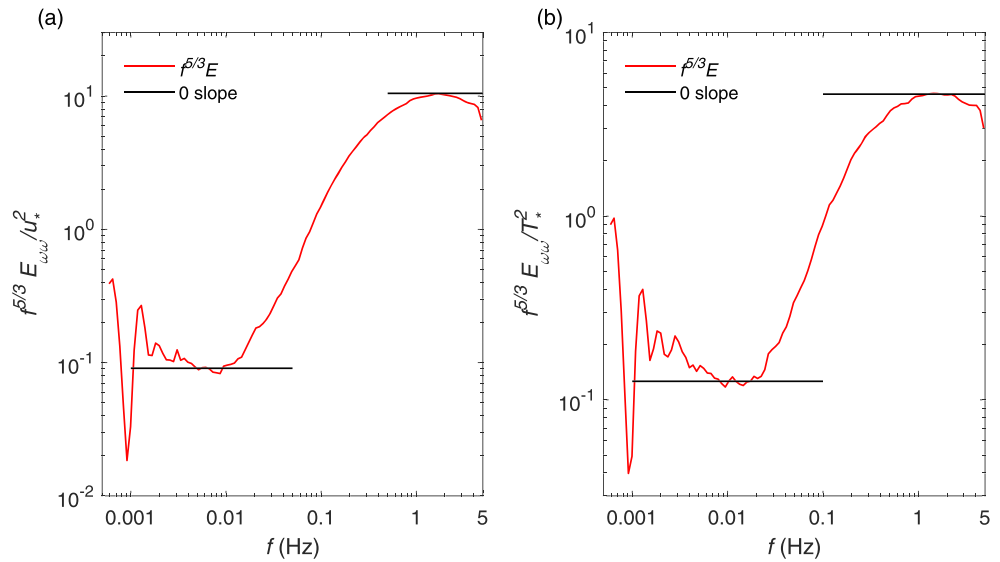


**Figure 6.** Median of compensated temporal wavelet spectra of (a) TKE and (b) temperature for each frequency in 60 representative 30-min periods of Dome C data.  $E_{\omega\omega}$  is wavelet spectrum in frequency,  $u_*$  is the friction velocity,  $T_*$  is the scaling temperature, and  $f$  is the sampling frequency.

region, there is not a universal power law scaling for spectra although the slope is less steep than  $-5/3$ . Our focus is the equilibrium range in the ABL so that the spectral slope at the energy-containing range is not shown.

When  $k_O > k_a$ , the width of the transition region denoted by the ratio of the buoyancy scale  $L_b$  to Dougherty-Ozmidov scale  $L_O$  increases with  $z/L$  (Figure 1b). Therefore, the transition region will play a more important role in more stable conditions, which then requires the consideration of  $L_b$  and  $L_O$  in turbulence parameterization. MOST (Monin & Obukhov, 1954) only applies two length scales to calculate turbulent fluxes, that is, the measurement height  $z$  (distance to the wall) and the Obukhov length  $L$  (Obukhov, 1946). In the case of  $k_O > k_a$ , the effects of measurement height  $z$  on stratified turbulence will be replaced by the Dougherty-Ozmidov scale  $L_O$ , thus leaving only the Obukhov length  $L$  effective in MOST. Grachev et al. (2015) showed that the ratio of  $L_O$  to  $L$  can be defined by the Prandtl number and flux Richardson number, so that the effects of  $L_O$  are inherently represented by MOST. However, the other characterizing

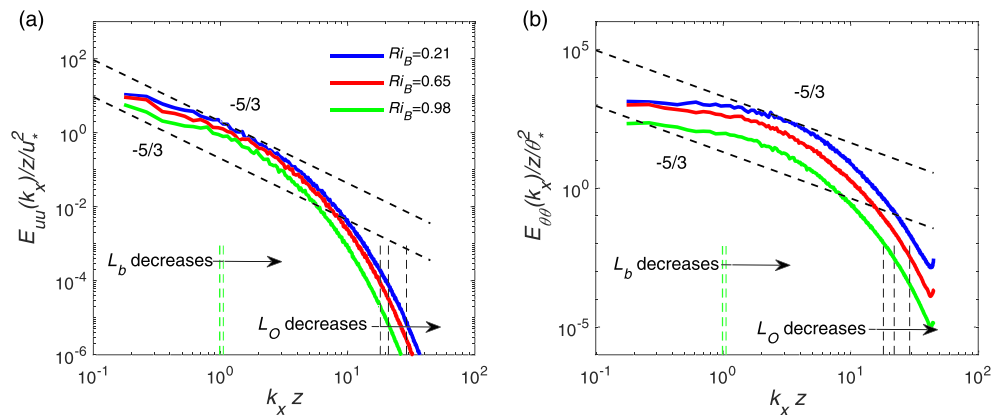


**Figure 7.** One-dimensional streamwise spectra scaled similarly to the observational data: (a) One-dimensional spectrum of streamwise velocity  $u$  in the streamwise direction. (b) One-dimensional spectrum of potential temperature  $\theta$  in the streamwise direction. Blue, red, and green lines indicate the spectra at  $ft = 0.02, 0.14,$  and  $0.20$  with respective increasing bulk  $Ri_B$  from 0.21, 0.65 to 0.98 taking at approximately  $z^+ = 65$  to fall in the inertial layer. The black dashed lines indicate the classic  $-5/3$  slope; the vertical green (black) dashed lines denote the scaled wavenumber corresponding to the decreasing buoyancy scale  $L_b$  (Dougherty-Ozmidov scale  $L_O$ ).  $k_x$  is the streamwise wavenumber,  $\theta_*$  is the scaling potential temperature, and other variables have the same meaning as those in Figure 2.

length scale  $L_b$  of the transition region is not considered in MOST and cannot be defined as a function of other MOST scales (Figure 1b), thus leading to the failure of MOST in calculating turbulent fluxes in very stable ABL ( $k_o > k_a$ ). And physically  $L_b$  denoting the thickness of the shear layers (Waite & Bartello, 2004) is another important length scale. Therefore, the buoyancy scale  $L_b$  has to be explicitly added to dimensional analysis of MOST in very stable conditions ( $k_o > k_a$ ). Besides, due to the increased impact of the transition region, the typically assumed  $-5/3$  spectral scaling (Kaimal et al., 1972) has to be revised to better represent TKE and temperature variance. In the limit of an extremely stable boundary layer, the transition region would occupy a very large fraction of the inertial subrange as  $L_o$  approaches the Kolmogorov scale  $\eta$ , which may be interpreted as a collapse of turbulence. However, such collapse of turbulence was not seen in our observations of the ABL even at Dome C.

### 3.4. Discussion

In Kaimal (1973), a  $-5/3$  power law scaling was shown in the spectra of  $u$ ,  $v$ , and  $w$  at high wavenumbers in the atmospheric observations and was approximated by an empirical formula. The shallower slope of spectra in the “transition region” between  $L_b$  and  $L_o$  was not reported. However, Figure 1 in Caughey (1977) showed a shallower slope in  $u$  and  $T$  spectra at lower frequency compared to the isotropic  $-5/3$  scaling frequency range at the height of 8 m. Such a shallower slope of spectra was not as obvious at heights of 46 and 91 m above the surface, at which the atmosphere was not as stable as at 8 m. So Figure 1 in Caughey (1977) actually showed the existence of a transition region to the left hand side of the isotropic  $-5/3$  scaling in log-log plots. The Dougherty-Ozmidov scale  $L_o$  and buoyancy scale  $L_b$  were not shown in the figures of Caughey (1977) so the importance of the two scales under stratification might have been overlooked at that time. Recently, Riley and Lindborg (2008) showed that some geophysical turbulence spectra under stratification at scales larger than  $L_o$  should not be explained by Kolmogorov's isotropic turbulence hypothesis. We further show that stratification influences the turbulence spectra at scales larger than  $L_o$  by observation and derivation. The “transition region” that is highlighted in our work was not emphasized in previous research such as in Riley and Lindborg (2008) or Lindborg (2006).

One may still argue that the  $-5/3$  scaling around  $L_b$  in our observation should be explained by Lindborg's anisotropic  $k_h^{-5/3}$  cascade (Lindborg, 2006). However, Waite (2011) pointed out that the  $k_h^{-5/3}$  cascade is driven by anisotropic eddies with horizontal scales much larger than  $L_b$ ; that is, Lindborg's stratified turbulence cascade is unlikely to hold for  $L_b$ . Besides, compared to free atmosphere motion, ABL turbulence is microscale motion with a length scale smaller than 20 km and a temporal scale less than 1 hr (Fiedler & Panofsky, 1970; Monin & Yaglom, 1975). In addition, Waite (2011) suggested that both  $L_b$  and  $L_o$  are much smaller than the energy-containing horizontal scale in stratified turbulence. That is, to say, scales around  $L_b$  or  $L_o$  are in the equilibrium range in the stable ABL, which supports our analysis for  $k_1$  spectra. Moreover, several numerical studies (Augier et al., 2015; Brethouwer et al., 2007; Maffioli & Davidson, 2016; Waite, 2011) reported a “spectral bump” around  $L_b$ , which is neither predicted nor explained by Lindborg's  $k_h^{-5/3}$  spectra of anisotropic turbulence hypothesis. These results also suggest that  $L_b$  is not in the energy-containing range in the horizontal direction and support our equilibrium range analysis.

Some hypotheses on the mechanisms causing the spectral shape are discussed below. Earlier studies (Lumley, 1964; Townsend, 1958) assumed that gravity waves might occur in turbulent flows under stratification. The existence of gravity waves has been confirmed by laboratory measurements of stably stratified open-channel flow (Komori et al., 1983) and homogeneous stratified shear turbulence in a wind tunnel (Keller & Van Atta, 2000), Lagrangian measurements below the ocean mixed layer in northeast Pacific (D'Asaro & Lien, 2000), and DNS of homogeneous stably stratified turbulence (Holt et al., 1992; Jacobitz et al., 2005; Métais & Herring, 1989), stably stratified turbulent channel flow (Garcia-Villalba & Del Alamo, 2011; Iida et al., 2002; Yeo et al., 2009; Zonta et al., 2012), and turbulent flow between two infinite horizontal plates (Moestam & Davidson, 2005), in particular at large scales (Garcia-Villalba & Del Alamo, 2011; Holt et al., 1992; Yeo et al., 2009; Zonta et al., 2012). The  $-5/3$  spectral slope at scales larger than  $L_b$  is related to a constant spectral energy transfer rate (see section 2.4.1), which is smaller than  $\epsilon_o$  in isotropic turbulence below  $L_o$ . However, the variation of spectral energy transfer rate in wavenumber leads to different spectral slopes in the transition region. Therefore, the different spectral characteristics between the buoyancy subrange and the transition region correspond to different interaction strengths between gravity waves and turbulence. The spectra shallower than  $-5/3$  in the transition region indicate extra energy between  $L_b$  and  $L_o$ . The extra energy might possibly come from potential energy that is converted to kinetic energy through countergradient heat flux (Holt et al., 1992; Jacobitz et al., 2005; Iida & Nagano, 2007;

Keller & Van Atta, 2000; Komori & Nagata, 1996; Komori et al., 1983; Schumann, 1987; Venayagamoorthy & Koseff, 2016; Zilitinkevich et al., 2007) in stratified turbulence. Another possible explanation of the shallower spectra might be Kelvin-Helmholtz instabilities (Brethouwer et al., 2007; Laval et al., 2003; Waite, 2011). In fact, Brethouwer et al. (2007) found countergradient fluxes appearing nearly simultaneously with Kelvin-Helmholtz-type instabilities. Therefore, further research are needed to explain the relation between the shallower spectra, countergradient fluxes, and Kelvin-Helmholtz instabilities.

A point worthy of discussion is the required resolution of LES in the stable ABL. Scale-invariant Smagorinsky subgrid-scale models already assume that the cutoff scale should be within the isotropic inertial subrange (Canuto & Cheng, 1997; Lilly, 1967). Other subgrid-scale models, for example, the scale-dependent Lagrangian dynamic model (Bou-Zeid et al., 2005), do not require that the cutoff size should fall in the isotropic inertial subrange. However, the resolved scale still needs to be below the Dougherty-Ozmidov scale in order to reproduce the proposed TKE spectrum in the equilibrium range. To strike a balance between the computational efficiency and accuracy, development of subgrid-scale stress models accounting for the spectral transition region and anisotropic turbulence could be a viable approach in the future.

#### 4. Conclusion

In the stable ABL, we showed for the first time that the TKE and temperature spectra in horizontal wavenumber consist of the buoyancy subrange, a transition region, and the isotropic inertial subrange in the equilibrium range. Those three regions are separated by  $k_b$  and  $\max(k_o, k_a)$ . The transition region between the buoyancy scale  $L_b$  and Dougherty-Ozmidov scale  $L_o$  can be observed when the conditions  $Fr_h^{1/2} \leq 1.118 \frac{v_m}{U} \ll 1$  and  $R_f < 0.25$  (for the existence of continuous turbulence with Richardson-Kolmogorov cascade) are satisfied. To represent the full spectra in horizontal wavenumber in the stably stratified ABL, LES would need to resolve scales as small as the  $L_o$  and use suitable subgrid-scale models. To correctly represent those regimes, DNS would have to be run at much higher Reynolds number to obtain larger-scale separation between  $L_o$  and the Kolmogorov scale  $\eta$ , as well as in the energy-containing range. The effects of the transition region on turbulent flux modeling have to be addressed; that is, the buoyancy scale  $L_b$  needs to be explicitly represented in MOST in very stable conditions at  $k_o > k_a$ .

#### Acknowledgments

P. G. would like to acknowledge funding from the National Science Foundation (NSF CAREER, EAR-1552304) and from the Department of Energy (DOE Early Career, DE-SC00142013). The lake data were collected by the Environmental Fluid Mechanics and Hydrology Laboratory of Professor M. Parlange at L'École Polytechnique Fédérale de Lausanne. We would like to thank Prof. M. Parlange and Prof. Elie Bou-Zeid for sharing Lake EC data and thank Prof. Jeffrey Basara for sharing MOISST EC data. The Dome C data were acquired in the frame of the projects "Mass lost in wind flux" (MALOX) and "Concordia multiprocess atmospheric studies" (COMPASS) sponsored by PNRA. A special thanks to P. Grigioni and all the staff of "Antarctic Meteorological Observatory" of Concordia for providing the radio sounding used in this study. And a special thanks to Dr. Igor Petenko of CNR ISAC for running the field experiment at Concordia station. We would also like to thank Prof. John Selker and Center for Transformative Environmental Monitoring Programs (CTEMPs) for help in the DTS experiment. We would like to acknowledge the National Center of Atmospheric Research computing facilities Yellowstone and Cheyenne where the DNS study was performed. The Dome C data can be downloaded from the <http://www.climantartide.it> website. Other data can be downloaded from the website (<https://doi.org/10.7916/d8-9vba-pn54>).

#### References

- Ansonge, C., & Mellado, J. P. (2014). Global intermittency and collapsing turbulence in the stratified planetary boundary layer. *Boundary-Layer Meteorology*, *153*(1), 89–116. <https://doi.org/10.1007/s10546-014-9941-3>
- Ansonge, C., & Mellado, J. P. (2016). Analyses of external and global intermittency in the logarithmic layer of Ekman flow. *Journal of Fluid Mechanics*, *805*, 611–635. <https://doi.org/10.1017/jfm.2016.534>
- Augier, P., Billant, P., & Chomaz, J. M. (2015). Stratified turbulence forced with columnar dipoles: Numerical study. *Journal of Fluid Mechanics*, *769*, 403–443. <https://doi.org/10.1017/jfm.2015.76>
- Baker, M. A., & Gibson, C. H. (1987). Sampling turbulence in the stratified ocean: Statistical consequences of strong intermittency. *Journal of Physical Oceanography*, *17*(10), 1817–1836. [https://doi.org/10.1175/1520-0485\(1987\)017<1817:STITSO>2.0.CO;2](https://doi.org/10.1175/1520-0485(1987)017<1817:STITSO>2.0.CO;2)
- Beare, R. J., Macvean, M. K., Holtslag, A. A., Cuxart, J., Esau, I., Golaz, J. C., et al. (2006). An intercomparison of large-eddy simulations of the stable boundary layer. *Boundary-Layer Meteorology*, *118*(2), 247–272. <https://doi.org/10.1007/s10546-004-2820-6>
- Billant, P., & Chomaz, J. M. (2001). Self-similarity of strongly stratified inviscid flows. *Physics of Fluids*, *13*(6), 1645–1651. <https://doi.org/10.1063/1.1369125>
- Biltoft, C. (2001). Some thoughts on local isotropy and the 4/3 lateral to longitudinal velocity spectrum ratio. *Boundary-Layer Meteorology*, *100*(3), 393–404. <https://doi.org/10.1023/A:1019289915930>
- Bolgiano, R. (1959). Turbulent spectra in a stably stratified atmosphere. *Journal of Geophysical Research*, *64*(12), 2226–2229. <https://doi.org/10.1029/JZ064i012p02226>
- Bou-Zeid, E., Meneveau, C., & Parlange, M. (2005). A scale-dependent Lagrangian dynamic model for large eddy simulation of complex turbulent flows. *Physics of Fluids*, *17*(2), 25105. <https://doi.org/10.1063/1.1839152>
- Bou-Zeid, E., Vercauteren, N., Parlange, M. B., & Meneveau, C. (2008). Scale dependence of subgrid-scale model coefficients: An a priori study. *Physics of Fluids*, *20*(11), 115106. <https://doi.org/10.1063/1.2992192>
- Bradley, E. F., Antonia, R., & Chambers, A. (1981). Turbulence Reynolds number and the turbulent kinetic energy balance in the atmospheric surface layer. *Boundary-Layer Meteorology*, *21*(2), 183–197. <https://doi.org/10.1007/BF02033936>
- Brethouwer, G., Billant, P., Lindborg, E., & Chomaz, J. M. (2007). Scaling analysis and simulation of strongly stratified turbulent flows. *Journal of Fluid Mechanics*, *585*, 343–368. <https://doi.org/10.1017/S0022112007006854>
- Canuto, V. M., & Cheng, Y. (1997). Determination of the Smagorinsky Lilly constant CS. *Physics of Fluids*, *9*(5), 1368–1378. <https://doi.org/10.1063/1.869251>
- Carnevale, G. F., Briscolini, M., & Orlandi, P. (2001). Buoyancy-to inertial-range transition in forced stratified turbulence. *Journal of Fluid Mechanics*, *427*, 205–239. <https://doi.org/10.1017/S002211200000241X>
- Caughey, S. (1977). Boundary-layer turbulence spectra in stable conditions. *Boundary-Layer Meteorology*, *11*(1), 3–14. <https://doi.org/10.1007/BF00221819>
- Chamecki, M., & Dias, N. (2004). The local isotropy hypothesis and the turbulent kinetic energy dissipation rate in the atmospheric surface layer. *Quarterly Journal of the Royal Meteorological Society*, *130*(603), 2733–2752. <https://doi.org/10.1256/qj.03.155>



- Cheng, Y., Parlange, M. B., & Brutsaert, W. (2005). Pathology of Monin-Obukhov similarity in the stable boundary layer. *Journal of Geophysical Research: Atmospheres*, *110*, D06101. <https://doi.org/10.1029/2004JD004923>
- Cheng, Y., Sayde, C., Li, Q., Basara, J., Selker, J., Tanner, E., & Gentine, P. (2017). Failure of Taylor's hypothesis in the atmospheric surface layer and its correction for eddy-covariance measurements. *Geophysical Research Letters*, *44*(9), 4287–4295. <https://doi.org/10.1002/2017GL073499>
- Cho, J. Y., & Lindborg, E. (2001). Horizontal velocity structure functions in the upper troposphere and lower stratosphere: 1. Observations. *Journal of Geophysical Research*, *106*(D10), 10,223–10,232. <https://doi.org/10.1029/2000JD900814>
- Chung, D., & Matheou, G. (2012). Direct numerical simulation of stationary homogeneous stratified sheared turbulence. *Journal of Fluid Mechanics*, *696*, 434–467. <https://doi.org/10.1017/jfm.2012.59>
- Coleman, G., Ferziger, J., & Spalart, P. (1992). Direct simulation of the stably stratified turbulent Ekman layer. *Journal of Fluid Mechanics*, *244*, 677–712. <https://doi.org/10.1017/S0022112092003264>
- D'Asaro, E. A., & Lien, R. C. (2000). Lagrangian measurements of waves and turbulence in stratified flows. *Journal of Physical Oceanography*, *30*(3), 641–655. [https://doi.org/10.1175/1520-0485\(2000\)030<0641:LMOWAT>2.0.CO;2](https://doi.org/10.1175/1520-0485(2000)030<0641:LMOWAT>2.0.CO;2)
- Dalaudier, F., & Sidi, C. (1990). Some characteristics of the turbulent buoyancy subrange. *Advances in Space Research*, *10*(10), 37–40. [https://doi.org/10.1016/0273-1177\(90\)90005-K](https://doi.org/10.1016/0273-1177(90)90005-K)
- Derbyshire, S. (1995). Stable boundary layers: Observations, models and variability part I: Modelling and measurements. *Boundary-Layer Meteorology*, *74*(1), 19–54. <https://doi.org/10.1007/BF00715709>
- Dougherty, J. (1961). The anisotropy of turbulence at the meteor level. *Journal of Atmospheric and Terrestrial Physics*, *21*(2-3), 210–213. [https://doi.org/10.1016/0021-9169\(61\)90116-7](https://doi.org/10.1016/0021-9169(61)90116-7)
- Fiedler, F., & Panofsky, H. A. (1970). Atmospheric scales and spectral gaps. *Bulletin of the American Meteorological Society*, *51*(12), 1114–1120. [https://doi.org/10.1175/1520-0477\(1970\)051<1114:ASASG>2.0.CO;2](https://doi.org/10.1175/1520-0477(1970)051<1114:ASASG>2.0.CO;2)
- Flores, O., & Riley, J. (2011). Analysis of turbulence collapse in the stably stratified surface layer using direct numerical simulation. *Boundary-Layer Meteorology*, *139*(2), 241–259. <https://doi.org/10.1007/s10546-011-9588-2>
- Gage, K., & Nastrom, G. (1986). Theoretical interpretation of atmospheric wavenumber spectra of wind and temperature observed by commercial aircraft during GASP. *Journal of the Atmospheric Sciences*, *43*(7), 729–740. [https://doi.org/10.1175/1520-0469\(1986\)043<0729:TIOAWS>2.0.CO;2](https://doi.org/10.1175/1520-0469(1986)043<0729:TIOAWS>2.0.CO;2)
- García-Villalba, M., & Del Alamo, J. C. (2011). Turbulence modification by stable stratification in channel flow. *Physics of Fluids*, *23*(4), 45104. <https://doi.org/10.1063/1.3560359>
- Gargett, A., Osborn, T., & Nasmyth, P. (1984). Local isotropy and the decay of turbulence in a stratified fluid. *Journal of Fluid Mechanics*, *144*, 231–280. <https://doi.org/10.1017/S0022112084001592>
- Gohari, S. I., & Sarkar, S. (2017). Direct numerical simulation of turbulence collapse and rebirth in stably stratified Ekman flow. *Boundary-Layer Meteorology*, *162*(3), 401–426. <https://doi.org/10.1007/s10546-016-0206-1>
- Grachev, A. A., Andreas, E. L., Fairall, C. W., Guest, P. S., & Persson, P. O. G. (2013). The critical Richardson number and limits of applicability of local similarity theory in the stable boundary layer. *Boundary-Layer Meteorology*, *147*(1), 51–82. <https://doi.org/10.1007/s10546-012-9771-0>
- Grachev, A. A., Andreas, E. L., Fairall, C. W., Guest, P. S., & Persson, P. O. G. (2015). Similarity theory based on the Dougherty–Ozmidov length scale. *Quarterly Journal of the Royal Meteorological Society*, *141*(690), 1845–1856. <https://doi.org/10.1002/qj.2488>
- Gulitski, G., Kholmyansky, M., Kinzelbach, W., Lüthi, B., Tsinober, A., & Yorish, S. (2007). Velocity and temperature derivatives in high-Reynolds-number turbulent flows in the atmospheric surface layer. Part I. Facilities, methods and some general results. *Journal of Fluid Mechanics*, *589*, 57–81. <https://doi.org/10.1017/S0022112007007495>
- He, P., & Basu, S. (2015). Direct numerical simulation of intermittent turbulence under stably stratified conditions. *Nonlinear Processes in Geophysics*, *22*(4), 447–471. <https://doi.org/10.5194/npg-22-447-2015>
- Herring, J. R., & Métais, O. (1989). Numerical experiments in forced stably stratified turbulence. *Journal of Fluid Mechanics*, *202*, 97–115.
- Holt, S. E., Koseff, J. R., & Ferziger, J. H. (1992). A numerical study of the evolution and structure of homogeneous stably stratified sheared turbulence. *Journal of Fluid Mechanics*, *237*, 499–539. <https://doi.org/10.1017/S0022112092003513>
- Horst, T. (1997). A simple formula for attenuation of eddy fluxes measured with first-order-response scalar sensors. *Boundary-Layer Meteorology*, *82*(2), 219–233. <https://doi.org/10.1023/A:1000229130034>
- Iida, O., Kasagi, N., & Nagano, Y. (2002). Direct numerical simulation of turbulent channel flow under stable density stratification. *International Journal of Heat and Mass Transfer*, *45*(8), 1693–1703. [https://doi.org/10.1016/S0017-9310\(01\)00271-X](https://doi.org/10.1016/S0017-9310(01)00271-X)
- Iida, O., & Nagano, Y. (2007). Effect of stable-density stratification on counter gradient flux of a homogeneous shear flow. *International Journal of Heat and Mass Transfer*, *50*(1-2), 335–347. <https://doi.org/10.1016/j.ijheatmasstransfer.2006.06.022>
- Jacobitz, F. G., Rogers, M. M., & Ferziger, J. H. (2005). Waves in stably stratified turbulent flow. *Journal of Turbulence*, *6*, N32. <https://doi.org/10.1080/14685240500462069>
- Jiménez, M., & Cuxart, J. (2005). Large-eddy simulations of the stable boundary layer using the standard Kolmogorov theory: Range of applicability. *Boundary-Layer Meteorology*, *115*(2), 241–261. <https://doi.org/10.1007/s10546-004-3470-4>
- Kaimal, J. C. (1973). Turbulence spectra, length scales and structure parameters in the stable surface layer. *Boundary-Layer Meteorology*, *4*(1-4), 289–309. <https://doi.org/10.1007/BF02265239>
- Kaimal, J. C., Wyngaard, J., Izumi, Y., & Coté, O. (1972). Spectral characteristics of surface-layer turbulence. *Quarterly Journal of the Royal Meteorological Society*, *98*(417), 563–589. <https://doi.org/10.1002/qj.49709841707>
- Katul, G. G., Li, D., Liu, H., & Assouline, S. (2016). Deviations from unity of the ratio of the turbulent Schmidt to Prandtl numbers in stratified atmospheric flows over water surfaces. *Physical Review Fluids*, *1*(3), 034401. <https://doi.org/10.1103/PhysRevFluids.1.034401>
- Katul, G. G., Porporato, A., & Nikora, V. (2012). Existence of k<sup>-1</sup> power-law scaling in the equilibrium regions of wall-bounded turbulence explained by Heisenberg's eddy viscosity. *Physical Review E*, *86*(6), 066311. <https://doi.org/10.1103/PhysRevE.86.066311>
- Katul, G. G., Porporato, A., Shah, S., & Bou-Zeid, E. (2014). Two phenomenological constants explain similarity laws in stably stratified turbulence. *Physical Review E*, *89*(2), 023007. <https://doi.org/10.1103/PhysRevE.89.023007>
- Keller, K. H., & Van Atta, C. W. (2000). An experimental investigation of the vertical temperature structure of homogeneous stratified shear turbulence. *Journal of Fluid Mechanics*, *425*, 1–29. <https://doi.org/10.1017/S0022112000002111>
- Khani, S., & Waite, M. L. (2014). Buoyancy scale effects in large-eddy simulations of stratified turbulence. *Journal of Fluid Mechanics*, *754*, 75–97. <https://doi.org/10.1017/jfm.2014.381>
- Kimura, Y., & Herring, J. (2012). Energy spectra of stably stratified turbulence. *Journal of Fluid Mechanics*, *698*, 19–50. <https://doi.org/10.1017/jfm.2011.546>
- Kolmogorov, A. N. (1941). The local structure of turbulence in incompressible viscous fluid for very large Reynolds numbers. *Doklady Akademii Nauk SSSR*, *30*(4), 299–303.

- Komori, S., & Nagata, K. (1996). Effects of molecular diffusivities on counter-gradient scalar and momentum transfer in strongly stable stratification. *Journal of Fluid Mechanics*, 326, 205–237. <https://doi.org/10.1017/S0022112096008294>
- Komori, S., Ueda, H., Ogino, F., & Mizushima, T. (1983). Turbulence structure in stably stratified open-channel flow. *Journal of Fluid Mechanics*, 130, 13–26. <https://doi.org/10.1017/S0022112083000944>
- Kunkel, G. J., & Marusic, I. (2006). Study of the near-wall-turbulent region of the high-Reynolds-number boundary layer using an atmospheric flow. *Journal of Fluid Mechanics*, 548, 375–402. <https://doi.org/10.1017/S0022112005007780>
- Lang, C., & Waite, M. L. (2019). Scale-dependent anisotropy in forced stratified turbulence. *Physical Review Fluids*, 4(4), 44801. <https://doi.org/10.1103/PhysRevFluids.4.044801>
- Laval, J. P., McWilliams, J. C., & Dubrulle, B. (2003). Forced stratified turbulence: Successive transitions with Reynolds number. *Physical Review E*, 68(3), 36308. <https://doi.org/10.1103/PhysRevE.68.036308>
- Li, D., & Bou-Zeid, E. (2011). Coherent structures and the dissimilarity of turbulent transport of momentum and scalars in the unstable atmospheric surface layer. *Boundary-Layer Meteorology*, 140(2), 243–262. <https://doi.org/10.1007/s10546-011-9613-5>
- Li, Q., Bou-Zeid, E., Vercauteren, N., & Parlange, M. (2018). Signatures of air–wave interactions over a large lake. *Boundary-Layer Meteorology*, 167(3), 445–468. <https://doi.org/10.1007/s10546-017-0329-z>
- Li, Q., Gentine, P., Mellado, J. P., & McColl, K. A. (2018). Implications of nonlocal transport and conditionally averaged statistics on Monin–Obukhov similarity theory and Townsend’s attached eddy hypothesis. *Journal of the Atmospheric Sciences*, 75(10), 3403–3431. <https://doi.org/10.1175/JAS-D-17-0301.1>
- Li, D., Katul, G. G., & Bou-Zeid, E. (2015). Turbulent energy spectra and cospectra of momentum and heat fluxes in the stable atmospheric surface layer. *Boundary-Layer Meteorology*, 157(1), 1–21. <https://doi.org/10.1007/s10546-015-0048-2>
- Li, D., Salesky, S. T., & Banerjee, T. (2016). Connections between the Ozmidov scale and mean velocity profile in stably stratified atmospheric surface layers. *Journal of Fluid Mechanics*, 797, R3. <https://doi.org/10.1017/jfm.2016.311>
- Lilly, D. K. (1967). The representation of small-scale turbulence in numerical simulation experiments. In *Proceedings of the IBM Scientific Computing Symposium on Environmental Sciences*, New York.
- Lilly, D. K. (1983). Stratified turbulence and the mesoscale variability of the atmosphere. *Journal of the Atmospheric Sciences*, 40(3), 749–761. [https://doi.org/10.1175/1520-0469\(1983\)040<0749:STATMV>2.0.CO;2](https://doi.org/10.1175/1520-0469(1983)040<0749:STATMV>2.0.CO;2)
- Lindborg, E. (2006). The energy cascade in a strongly stratified fluid. *Journal of Fluid Mechanics*, 550, 207–242. <https://doi.org/10.1017/S0022112005008128>
- Lumley, J. L. (1964). The spectrum of nearly inertial turbulence in a stably stratified fluid. *Journal of the Atmospheric Sciences*, 21(1), 99–102.
- Lumley, J. L. (1965). Theoretical aspects of research on turbulence in stratified flows. In *Atmospheric Turbulence and Radio Wave Propagation*, Nauka, Moscow, pp. 105–110.
- Lumley, J. L., & Panofsky, H. A. (1964). *The structure of atmospheric turbulence*. New York: John Wiley.
- Maffioli, A., & Davidson, P. (2016). Dynamics of stratified turbulence decaying from a high buoyancy Reynolds number. *Journal of Fluid Mechanics*, 786, 210–233. <https://doi.org/10.1017/jfm.2015.667>
- Mahrt, L. (1998). Stratified atmospheric boundary layers and breakdown of models. *Theoretical and Computational Fluid Dynamics*, 11(3), 263–279. <https://doi.org/10.1007/s001620050093>
- Mahrt, L. (1999). Stratified atmospheric boundary layers. *Boundary-Layer Meteorology*, 90(3), 375–396. <https://doi.org/10.1023/A:1001765727956>
- Mahrt, L. (2014). Stably stratified atmospheric boundary layers. *Annual Review of Fluid Mechanics*, 46, 23–45. <https://doi.org/10.1146/annurev-fluid-010313-141354>
- Massman, W. (2000). A simple method for estimating frequency response corrections for eddy covariance systems. *Agricultural and Forest Meteorology*, 104(3), 185–198. [https://doi.org/10.1016/S0168-1923\(00\)00164-7](https://doi.org/10.1016/S0168-1923(00)00164-7)
- Massman, W., & Lee, X. (2002). Eddy covariance flux corrections and uncertainties in long-term studies of carbon and energy exchanges. *Agricultural and Forest Meteorology*, 113(1), 121–144. [https://doi.org/10.1016/S0168-1923\(02\)00105-3](https://doi.org/10.1016/S0168-1923(02)00105-3)
- McComb, W. D., Berera, A., Salewski, M., & Yoffe, S. (2010). Taylor’s (1935) dissipation surrogate reinterpreted. *Physics of Fluids*, 22(6), 61704. <https://doi.org/10.1063/1.3450299>
- Mellado, J. P., van Heerwaarden, C. C., & Garcia, J. R. (2016). Near-surface effects of free atmosphere stratification in free convection. *Boundary-Layer Meteorology*, 159(1), 69–95. <https://doi.org/10.1007/s10546-015-0105-x>
- Métais, O., & Herring, J. R. (1989). Numerical simulations of freely evolving turbulence in stably stratified fluids. *Journal of Fluid Mechanics*, 202, 117–148. <https://doi.org/10.1017/S0022112089001126>
- Moestam, R., & Davidson, L. (2005). Numerical simulations of a thermocline in a pressure-driven flow between two infinite horizontal plates. *Physics of Fluids*, 17(7), 75109. <https://doi.org/10.1063/1.1920648>
- Monin, A., & Obukhov, A. (1954). Basic laws of turbulent mixing in the surface layer of the atmosphere. *Contributions to Geophysical Institute, Slovak Academy of Sciences USSR*, 151(163), e187.
- Monin, A., & Yaglom, A. (1975). *Statistical fluid mechanics: Mechanics of turbulence* (pp. 874). Cambridge, Massachusetts: MIT Press.
- Muschinski, A., Frehlich, R. G., & Balsley, B. B. (2004). Small-scale and large-scale intermittency in the nocturnal boundary layer and the residual layer. *Journal of Fluid Mechanics*, 515, 319–351. <https://doi.org/10.1017/S0022112004000412>
- Nastrom, G., & Gage, K. S. (1985). A climatology of atmospheric wavenumber spectra of wind and temperature observed by commercial aircraft. *Journal of the Atmospheric Sciences*, 42(9), 950–960. [https://doi.org/10.1175/1520-0469\(1985\)042<0950:ACOAWS>2.0.CO;2](https://doi.org/10.1175/1520-0469(1985)042<0950:ACOAWS>2.0.CO;2)
- Nieuwstadt, F. T. (1984). The turbulent structure of the stable, nocturnal boundary layer. *Journal of the Atmospheric Sciences*, 41(14), 2202–2216. [https://doi.org/10.1175/1520-0469\(1984\)041<2202:TTSOTS>2.0.CO;2](https://doi.org/10.1175/1520-0469(1984)041<2202:TTSOTS>2.0.CO;2)
- Obukhov, A. (1946). Turbulence in thermally inhomogeneous atmosphere. *The Institute of Theoretical Geophysics of the Academy of Sciences of the U.S.S.R.*, 1, 95–115.
- Ozmidov, R. (1965). On the turbulent exchange in a stably stratified ocean. *Izv. Acad. Sci. USSR. Atmospheric and Oceanic Physics*, 1, 861–871.
- Petenko, I., Argentini, S., Casasanta, G., Genthon, C., & Kallistratova, M. (2019). Stable surface-based turbulent layer during the polar winter at Dome C, Antarctica: Sodar and in situ observations. *Boundary-Layer Meteorology*, 171(1), 101–128. <https://doi.org/10.1007/s10546-018-0419-6>
- Phillips, O. M. (1965). On the Bolgiano and Lumley-Shur theories of the buoyancy subrange. In A. M. Yaglom & V. I. Tatarsky (Eds.), *Atmospheric Turbulence and Radio Wave Propagation* (pp. 121–128). Moscow: Nauka.
- Pope, S. (2000). *Turbulent flows*. Cambridge: Cambridge University Press. <https://doi.org/10.1017/CBO9780511840531>
- Riley, J. J., & DeBruynkops, S. M. (2003). Dynamics of turbulence strongly influenced by buoyancy. *Physics of Fluids*, 15(7), 2047–2059. <https://doi.org/10.1063/1.1578077>

- Riley, J. J., & Lindborg, E. (2008). Stratified turbulence: A possible interpretation of some geophysical turbulence measurements. *Journal of the Atmospheric Sciences*, *65*(7), 2416–2424. <https://doi.org/10.1175/2007JAS2455.1>
- Schumann, U. (1987). The countergradient heat flux in turbulent stratified flows. *Nuclear Engineering and Design*, *100*(3), 255–262. [https://doi.org/10.1016/0029-5493\(87\)90078-1](https://doi.org/10.1016/0029-5493(87)90078-1)
- Schumann, U., & Gerz, T. (1995). Turbulent mixing in stably stratified shear flows. *Journal of Applied Meteorology*, *34*(1), 33–48. <https://doi.org/10.1175/1520-0450-34.1.33>
- Selker, J., van de Giesen, N., Westhoff, M., Luxemburg, W., & Parlange, M. B. (2006). Fiber optics opens window on stream dynamics. *Geophysical Research Letters*, *33*, L24401. <https://doi.org/10.1029/2006GL027979>
- Shah, S. K., & Bou-Zeid, E. (2014). Direct numerical simulations of turbulent Ekman layers with increasing static stability: Modifications to the bulk structure and second-order statistics. *Journal of Fluid Mechanics*, *760*, 494–539. <https://doi.org/10.1017/jfm.2014.597>
- Sidi, C., & Dalaudier, F. (1989). Temperature and heat flux spectra in the turbulent buoyancy subrange. *Pure and Applied Geophysics*, *130*(2), 547–569. <https://doi.org/10.1007/BF00874474>
- Smedman, A. S. (1988). Observations of a multi-level turbulence structure in a very stable atmospheric boundary layer. *Boundary-Layer Meteorology*, *44*(3), 231–253. <https://doi.org/10.1007/BF00116064>
- Smeets, C., Duynkerke, P., & Vugts, H. (1998). Turbulence characteristics of the stable boundary layer over a mid-latitude glacier. Part I: A combination of katabatic and large-scale forcing. *Boundary-Layer Meteorology*, *87*(1), 117–145. <https://doi.org/10.1023/A:1000860406093>
- Smyth, W. D., & Moum, J. N. (2000). Length scales of turbulence in stably stratified mixing layers. *Physics of Fluids*, *12*(6), 1327–1342. <https://doi.org/10.1063/1.870385>
- Spalart, P. R., Coleman, G. N., & Johnstone, R. (2008). Direct numerical simulation of the Ekman layer: A step in Reynolds number, and cautious support for a log law with a shifted origin (Retracted article. See vol. 21, art. no. 109901, 2009). *Physics of Fluids*, *20*(10), 101507.
- Sreenivasan, K. R. (1984). On the scaling of the turbulence energy dissipation rate. *Physics of Fluids*, *27*(5), 1048–1051. <https://doi.org/10.1063/1.864731>
- Sreenivasan, K. R. (1995). On the universality of the Kolmogorov constant. *Physics of Fluids*, *7*(11), 2778–2784. <https://doi.org/10.1063/1.868656>
- Stull, R. B. (1988). An introduction to boundary layer meteorology, *13*. <https://doi.org/10.1007/978-94-009-3027-8>
- Sullivan, P. P., Weil, J. C., Patton, E. G., Jonker, H. J., & Mironov, D. V. (2016). Turbulent winds and temperature fronts in large-eddy simulations of the stable atmospheric boundary layer. *Journal of the Atmospheric Sciences*, *73*(4), 1815–1840. <https://doi.org/10.1175/JAS-D-15-0339.1>
- Taylor, G. I. (1935). Statistical theory of turbulence. *Proceedings of the Royal Society of London. Series A, Mathematical and Physical Sciences*, *151*(873), 421–478. <https://doi.org/10.1098/rspa.1935.0161>
- Taylor, G. I. (1938). The spectrum of turbulence. In *Proceedings of the Royal Society of London A: Mathematical, Physical and Engineering Sciences*, *164*, pp. 476–490. <https://doi.org/10.1098/rspa.1938.0032>
- Tong, C., & Ding, M. (2019). Multi-point Monin–Obukhov similarity in the convective atmospheric surface layer using matched asymptotic expansions. *Journal of Fluid Mechanics*, *864*, 640–669. <https://doi.org/10.1017/jfm.2019.38>
- Tong, C., & Nguyen, K. X. (2015). Multipoint Monin–Obukhov similarity and its application to turbulence spectra in the convective atmospheric surface layer. *Journal of the Atmospheric Sciences*, *72*(11), 4337–4348. <https://doi.org/10.1175/JAS-D-15-0134.1>
- Torrence, C., & Compo, G. P. (1998). A practical guide to wavelet analysis. *Bulletin of the American Meteorological Society*, *79*(1), 61–78. [https://doi.org/10.1175/1520-0477\(1998\)079<0061:APGTWA>2.0.CO;2](https://doi.org/10.1175/1520-0477(1998)079<0061:APGTWA>2.0.CO;2)
- Townsend, A. (1958). Turbulent flow in a stably stratified atmosphere. *Journal of Fluid Mechanics*, *3*(4), 361–372. <https://doi.org/10.1017/S0022112058000045>
- Townsend, A. (1976). *The structure of turbulent shear flow*. Cambridge: Cambridge University Press.
- Tulloch, R., & Smith, K. (2006). A theory for the atmospheric energy spectrum: Depth-limited temperature anomalies at the tropopause. *Proceedings of the National Academy of Sciences*, *103*(40), 14,690–14,694. <https://doi.org/10.1073/pnas.0605494103>
- Tyler, S. W., Selker, J. S., Hausner, M. B., Hatch, C. E., Torgersen, T., Thodal, C. E., & Schladow, S. G. (2009). Environmental temperature sensing using Raman spectra DTS fiber-optic methods. *Water Resources Research*, *45*, W00D23. <https://doi.org/10.1029/2008WR007052>
- Venayagamoorthy, S. K., & Koseff, J. R. (2016). On the flux Richardson number in stably stratified turbulence. *Journal of Fluid Mechanics*, *798*, R1. <https://doi.org/10.1017/jfm.2016.340>
- Vercauteren, N., Bou-Zeid, E., Parlange, M. B., Lemmin, U., Huwald, H., Selker, J., & Meneveau, C. (2008). Subgrid-scale dynamics of water vapour, heat, and momentum over a lake. *Boundary-Layer Meteorology*, *128*(2), 205–228. <https://doi.org/10.1007/s10546-008-9287-9>
- Vignon, E., Genthon, C., Barral, H., Amory, C., Picard, G., Gallée, H., et al. (2017). Momentum and heat-flux parametrization at Dome C, Antarctica: A sensitivity study. *Boundary-Layer Meteorology*, *162*(2), 341–367. <https://doi.org/10.1007/s10546-016-0192-3>
- Vignon, E., van de Wiel, B. J., van Hooijdonk, I. G., Genthon, C., van der Linden, S. J., van Hooft, J. A., et al. (2017). Stable boundary-layer regimes at Dome C, Antarctica: Observation and analysis. *Quarterly Journal of the Royal Meteorological Society*, *143*(704), 1241–1253. <https://doi.org/10.1002/qj.2998>
- Waite, M. L. (2011). Stratified turbulence at the buoyancy scale. *Physics of Fluids*, *23*(6), 66602. <https://doi.org/10.1063/1.3599699>
- Waite, M. L. (2014). Direct numerical simulations of laboratory-scale stratified turbulence. In *Modelling Atmospheric and Oceanic Flows: Insights from Laboratory Experiments* (T. von Larcher, & P. Williams, Eds.), American Geophysical Union. <https://doi.org/10.1002/9781118856024.ch8>
- Waite, M. L., & Bartello, P. (2004). Stratified turbulence dominated by vortical motion. *Journal of Fluid Mechanics*, *517*, 281–308. <https://doi.org/10.1017/S0022112004000977>
- Waite, M. L., & Bartello, P. (2006). Stratified turbulence generated by internal gravity waves. *Journal of Fluid Mechanics*, *546*, 313–339. <https://doi.org/10.1017/S0022112005007111>
- Weinstock, J. (1976). Nonlinear theory of acoustic-gravity waves 1. Saturation and enhanced diffusion. *Journal of Geophysical Research*, *81*(4), 633–652. <https://doi.org/10.1029/JA081i004p00633>
- Weinstock, J. (1978). On the theory of turbulence in the buoyancy subrange of stably stratified flows. *Journal of the Atmospheric Sciences*, *35*(4), 634–649. [https://doi.org/10.1175/1520-0469\(1978\)035<0634:OTTOTI>2.0.CO;2](https://doi.org/10.1175/1520-0469(1978)035<0634:OTTOTI>2.0.CO;2)
- Yeo, K., Kim, B. G., & Lee, C. (2009). Eulerian and Lagrangian statistics in stably stratified turbulent channel flows. *Journal of Turbulence*, *10*(N17), 1–26. <https://doi.org/10.1080/14685240902902365>
- Zilitinkevich, S., Elperin, T., Kleerorin, N., & Rogachevskii, I. (2007). Energy and flux-budget (EFB) turbulence closure model for stably stratified flows. Part I: Steady-state, homogeneous regimes. *Boundary-Layer Meteorology*, *125*(2), 167–191. <https://doi.org/10.1007/s10546-007-9189-2>

- Zilitinkevich, S., Elperin, T., Kleorin, N., Rogachevskii, I., & Esau, I. (2013). A hierarchy of energy-and flux-budget (EFB) turbulence closure models for stably-stratified geophysical flows. *Boundary-Layer Meteorology*, *146*(3), 341–373. <https://doi.org/10.1007/s10546-012-9768-8>
- Zonta, F., Onorato, M., & Soldati, A. (2012). Turbulence and internal waves in stably-stratified channel flow with temperature-dependent fluid properties. *Journal of Fluid Mechanics*, *697*, 175–203. <https://doi.org/10.1017/jfm.2012.51>